Journal of Theoretical Biology 498 (2020) 110294

Contents lists available at ScienceDirect

Journal of Theoretical Biology

journal homepage: www.elsevier.com/locate/jtb

Electric discharge of electrocytes: Modelling, analysis and simulation

Zilong Song[a], Xiulei Cao[b], Tzyy-Leng Horng[c], Huaxiong Huang[d,b,e,*]

[a] Department of Mathematics, University of California, Riverside, CA 92521, U.S.A.
[b] Department of Mathematics & Statistics, York University, Toronto, Ontario M3J 1P3, Canada
[c] Department of Applied Mathematics, Feng Chia University, Taichung 40724, Taiwan
[d] BNU-UIC Joint Mathematical Research Centre, Zhuhai, Guangdong 519087, China
[e] Department of Computer Science, University of Toronto, Toronto, Ontario M5T 3A1, Canada

ARTICLE INFO

Article history:
Received 12 February 2020
Revised 17 April 2020
Accepted 20 April 2020
Available online 27 April 2020

Keywords:
Electrocytes
Electric discharge
Poisson-Nernst-Planck system
Asymptotic analysis
Numerical simulation

ABSTRACT

In this paper, we investigate the electric discharge of electrocytes by extending our previous work on the generation of electric potential. We first give a complete formulation of a single cell unit consisting of an electrocyte and a resistor, based on a Poisson-Nernst-Planck (PNP) system with various membrane currents as interfacial conditions for the electrocyte and a Maxwell's model for the resistor. Our previous work can be treated as a special case with an infinite resistor (or open circuit). Using asymptotic analysis, we simplify our PNP system and reduce it to an ordinary differential equation (ODE) based model. Unlike the case of an infinite resistor, our numerical simulations of the new model reveal several distinct features. A finite current is generated, which leads to non-constant electric potentials in the bulk of intracellular and extracellular regions. Furthermore, the current induces an additional action potential (AP) at the non-innervated membrane, contrary to the case of an open circuit where an AP is generated only at the innervated membrane. The voltage drop inside the electrocyte is caused by an internal resistance due to mobile ions. We show that our single cell model can be used as the basis for a system with stacked electrocytes and the total current during the discharge of an electric eel can be estimated by using our model.

1. Introduction

Electric eels (*Electrophorus electricus*) have fascinated both scientists and the public for centuries (Carlson, 2015; Moller, 1995; Campenot, 2016). They are well-known for using electricity in various remarkable ways to track and immobilize prey and defend themselves from predators (Bauer, 1979; Westby, 1988; Nelson et al., 2016). The written account of their special capability dated back to 1500s even before the knowledge of electricity, and its connection with electricity was hypothesized in the 1700s (Finger and Piccolino, 2011). They also played a crucial role in the discovery of electricity in the nervous system and muscles (Finger and Piccolino, 2011; Campenot, 2016).

Since the 1950s, there have been a number of experiments on electric eels to investigate the electrogenic mechanisms and the functions of electric discharge (Keynes and Martins-Ferreira, 1953; Maciver et al., 2001; Markham, 2013; Lissmann, 1958), and particularly there has been a resurgent of interest in the last decade motivated by a series of excellent experiments conducted by Catania (2014, 2015a, 2015b, 2017a). Eels can produce both low intensity and high intensity electric fields for tracking and attacking the prey to active sensing and communication (Carlson, 2015; Catania, 2015b). It is reported (Brown, 1950; Coates, 1950; Catania, 2017a) that large eels can produce electric fields with magnitude up to 600 V, and when in contact with the prey, an external current as high as 1 A can be generated, which is lethal to many animals. Catania (2014, 2015c) showed that eels can immobilize a prey or detect its location over a certain distance, by activating prey motor neurons with distinct types of discharges. To model the defensive leaping behaviour, an equivalent circuit (Catania, 2017a; 2017b), was proposed. It shows that a high voltage is generated when the eel is connected to an insulator and an electric discharge with high current develops when the eel makes a contact with a conductor (Catania, 2016).

The electric discharge is generated by an identifiable electric organ (Markham, 2013), which makes up about 80% of the eel's body and consists of thousands of electrocytes. Stacked electrocytes behave like stacked mini batteries to produce the high voltage (Gotter et al., 1998; Mauro, 1969). The electrogenic mechanism

* Corresponding author.
E-mail addresses: hhuang@uic.edu.hk, hhuang@yorku.ca (H. Huang).

https://doi.org/10.1016/j.jtbi.2020.110294
0022-5193/

of each electrocyte is closely related to ion transport across the membrane and the firing of action potentials (APs) (Keynes and Martins-Ferreira, 1953; Gotter et al., 1998; Dunlap et al., 1997). The electrocyte has cell polarity and possesses two primary membranes, innervated and non-innervated membranes, where various types of ion channels, receptors and pumps abound and allow ionic currents through them (Xu and Lavan, 2008; Sheridan and Lester, 1977; Noda et al., 1984). The firing of APs at innervated membrane is similar to that in the nerve cells, and results in the transcellular potential difference (~ 0.15 V).

Electrocytes can be thought of as many electric cells in series consisting of capacitor (innervated and non-innervated membranes) and conductor (electrolyte) in series. It can store electric charges and discharge electric current. The energy is transported from bioenergy to electric energy when charging (polarizing) through pumps and active transporters on membranes, which uses ATP to build up and maintain concentration gradient of ions across membrane. The mechanism of electrocytes has inspired many applications in other scientific fields, particularly it has been mimicked to design and manufacture artificial batteries. It has been exploited to design promising power source for medical devices by using synthetic cells (Xu and Lavan, 2008; Humayun et al., 2003). The mechanism has also been mimicked by using stacked hydrogels (Schroeder et al., 2017) to generate biocompatible electric power source for implant materials. Another study (Sun et al., 2016) shows that a stretchy fibre that mimics electric eels could power wearable electronic devices, where alternating segments of conductive carbon nanotubes and insulating elastic rubbers coated with electrolyte gel are used.

For an electrocyte, ODE (membrane) models are often utilized to study membrane excitability and high voltage generation (Xu and Lavan, 2008; Gotter et al., 1998). The ionic currents through membranes are often described by distinct models for various ion channels and receptors, including the celebrated Hodgkin-Huxley (HH) model (Hodgkin and Huxley, 1990). The HH model was first utilized to study APs in squid giant axon (Hodgkin and Huxley, 1952), and hence could be extended to study the innervated membrane of electrocyte. Xu and Lavan (2008) have proposed a membrane model by taking into account both innervated and non-innervated membranes, and a superposition of the two membrane potentials leads to the final transcellular potential difference. In these membrane models, ionic concentrations and electric potential are assumed to be constants in the extracellular (EC) and intracellular (IC) regions, and the boundary layer (BL) or electric double layer is neglected.

Our previous work (Cao et al., 2019) applied the Poisson-Nernst-Planck (PNP) formulation to an electrocyte with various membrane currents as interfacial conditions at the membranes, focusing on the mechanism of voltage generation. The membrane model (Xu and Lavan, 2008) can be derived from the PNP formulation as a leading-order approximation by asymptotic analysis. The PNP system has found great success in modeling ion transport in cells and ion channels (Rubinstein, 1990; Mori et al., 2011; Liu, 2009; Liu and Eisenberg, 2014; Schmuck and Bazant, 2015; Pods, 2017), as well as AP propagation in axons (Pods et al., 2013; Song et al., 2018a). We did not consider the scenario when the electric eel and the prey form a closed electric circuit, where the eel functions as a battery and the prey is interpreted as a resistor. The complication lies in the transient nature of the system, when the current goes through the electrocyte and the resistor. As stated in the Maxwell's equations Jackson (1999), the total current (Eisenberg et al., 2017; 2018) consists of both current induced by the ions and the time variation of electric field, i.e., $\epsilon\partial_t E$. This induced current $\epsilon\partial_t E$ becomes important when complicated forms of current appear in the circuit, and ensures that the total current is conserved in a closed circuit. This term has also found importance in electronic circuits of computers (Horowitz and Hill, 2015; Eisenberg et al., 2017), related to stay capacitance.

It is desirable to investigate the discharge of electric eels through a PDE model (here called PNP+resistor model), which we believe is a more fundamental formulation than the ODE (membrane) model. In the PDE approach, the spacial information is not neglected. First, there is cell polarity for the electrocyte where pumps, channels and transporters are not homogeneously distributed on the membranes, so one needs to treat the innervated and non-innervated membranes separately. Second, this work considers a series of stacked electrocytes, and one needs to upscale the model for one electrocyte structure to a macroscopic model. Third, it is essential to capture the spacial variation of electric potential in IC and EC spaces and the BLs near the membranes and the junction of electrocyte and resistor. It allows us to identify the induced current due to the transient nature of the electric fields, a combination of spatial-temporal effects. Another benefit of PDE model is that the total current in the system can be naturally defined and preserved for the whole system.

In this paper, we study electric discharge of electrocytes by extending our previous work on open circuit (electrocyte+infinite resistor) to the case of closed circuit (electrocyte+finite resistor). We first give a complete formulation for a single cell unit consisting of the electrocyte and resistor, where PNP system is combined with various membrane currents and a model for the resistor. The total current for the system is suitably defined, which includes the $\epsilon\partial_t E$ term and is conserved in the system. With the definition of total current, it is natural to recover the classical membrane models for membrane potentials in general cases. A boundary layer (BL) is present at the junction of electrocyte and resistor, since the current transit from one form to the other. Using asymptotic analysis, we derive a membrane (ODE) model for the closed circuit. Numerical simulations are carried out to make comparison between PNP and membrane models and to capture distinct features of the closed circuit. Finite current is observed in the closed circuit, and BLs near membrane and the junctions are confirmed. Unlike the open circuit case, the finite current leads to non-constant electric potential in the intracellular (IC) and extracellular (EC) spaces, and it induces an AP at the non-innervated membrane. The voltage drop in bulk of electrocyte is due to the internal resistance, reflected by the equivalent conductance/resistance defined by concentrations. We also show how total current of an electric eel can be estimated by using our single cell model, which is consistent to the values from experiments reported in the literature.

The manuscript is arranged as follows. Section 2 presents the "PNP+ resistor" model for a mini structure of electrocyte and resistor, with the total current suitably defined. Asymptotic analysis is performed in Section 3, to analyze the basic features and to derive an ODE model for the closed circuit. Section 4 is devoted to the numerical simulations of the PNP and ODE models, where the features including BLs are confirmed and the total current is estimated. Finally, concluding remarks are provided in Section 5.

2. Problem formulation

The electric organ of an electric eel consists of thousands of electrocytes, each functions as a mini battery. When the eel attacks a prey, there are two possibilities. In the first scenario, before the contact is made with the prey, each electrocyte is fired simultaneously and a significant electric potential can be built up on the organ scale by adding the potential difference from each cell, which is the subject of our previous paper Cao et al. (2019). In the second scenario, the contact is made with the prey when the electrocytes are activated. In this case, we need to include the prey in our model. Fig. 1(a) illustrates the two-dimensional view of stacked electrocytes in electric organ and the one-dimensional (1D)

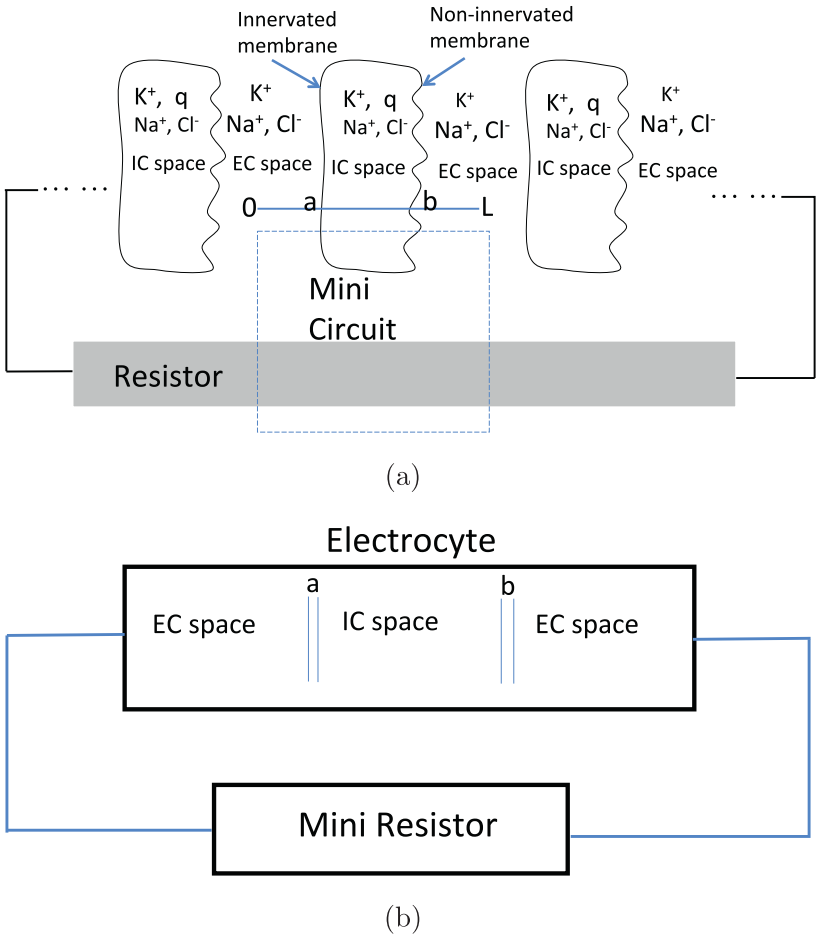

Fig. 1. Sketch of electric circuits for electric discharge of eels (a) stacked electrocytes from electric organ and the external resistor (i.e., the prey), (b) mini closed circuit with one electrocyte and mini resistor, where EC and IC stand for extracellular and intracellular respectively.

electric circuit where the electric organ plays the role of battery and the prey is an equivalent external resistor (see also Keynes and Martins-Ferreira (1953); Gotter et al. (1998)). A mini-circuit model is first considered as shown in 1(b), which consists of one electrocyte and one external mini-resistor. After the analysis and justification of the mini-circuit model by PNP model, we will provide the connection to the macroscopic circuit model by approximately the superposition principle.

2.1. A mini closed circuit

We consider a small scale 1D closed circuit, which consists of a unit structure of electrocyte (like a battery) and a mini-resistor, as shown in Fig. 1(b). The interior of the electrocyte is separated from the EC spaces by two membranes, acting as capacitors. The EC space of the electrocyte is connected to a mini-resistor (part of prey). In a real battery-resistor circuit, the electric potential (V) of the battery drives a current (I) through the resistor (R), and we have the Ohm's law $V = IR$. In the case of an electrocyte, the situation is more complicated. First of all, the electric potential needs to be generated when the ion channels on the membranes are activated. In general, it can be described using the following dynamic equation (e.g., Hodgkin-Huxley model)

$$C_m \frac{dV_m^a}{dt} + I_{channel} = I^*, \tag{1}$$

where C_m is the membrane capacitance, V_m^a is the membrane potential at membrane a (intracelluar potential minus extracellular potential), $I_{channel}$ denotes various current through ion channels on membrane, and I^* is the total current in the circuit. A similar equation applies to membrane potential V_m^b at membrane b. Roughly speaking, the superposition of the two membrane potential provides the total voltage V and the total current is the same $I^* = I$ in an electric circuit. More accurately for the resistor, according to the Maxwell equation (Eisenberg et al., 2018), the total current I^* consists of two components: I and $\epsilon \partial_t E$ (induced current) where E is electric field. When the total current passes through the closed circuit, we must have

$$V_m^a - V_m^b = V. \tag{2}$$

In the following, we wish to address a few questions. The main question is whether this is a consistent model. One aspect is whether the model is consistent with a more detailed PNP+resistor model (considered as a more fundamental model) and retains all the essential features through reduction. The other aspect is whether the model prediction is consistent with experimental observations. A related issue is how to compute V_{ma}, V_{mb} and I^*. The final question is how to validate our one electrocyte mini-circuit model with experimental observations such as voltage and current coming from a system with many electrocytes, i.e., to derive a macroscopic circuit model.

2.2. PNP+resistor model

As in Figs. 1 and 2, we treat the unit structure of electrocyte as a 1D structure. The electrocyte consists of IC and EC spaces, separated by two primary membranes, one innervated at $x = a$ and

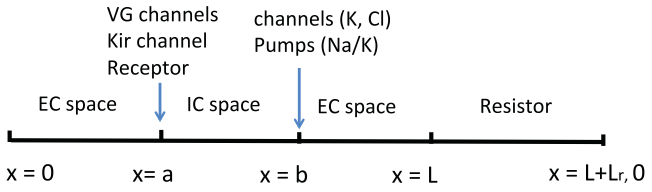

Fig. 2. The 1D setup for the PNP+resistor model.

the other non-innervated at $x = b$. Various transmembrane proteins, such as channels and pumps, are asymmetrically distributed across the two membranes, which allow ionic currents through the membranes. Three major ions (called bio-ions) Na^+, K^+ and Cl^- are considered, as they are the most relevant in the setting of electric discharge by electrocytes.

Poisson-Nernst-Planck (PNP) system is widely accepted to describe the ion transport in cells, and it has been proved to be accurate for dilute ionic solutions (Kilic et al., 2007a; 2007b; Song et al., 2019). For electrocytes, all the ionic concentrations in EC and IC spaces are at most at the scale of 100 mM (see Eq. (12)), which is roughly $O(10^{-3})$ of maximum ionic concentrations determined by ionic radius (Song et al., 2019), so they can be treated as dilute ionic solutions. Therefore, the transport of the three major ions in the EC and IC spaces are modelled by the PNP system. Ionic currents through the membranes are described by various empirical or experimental models, depending on the types of transmembrane proteins involved. A general model for the resistor based on Maxwell's equation are adopted, and suitable connection conditions are proposed at junctions to form an electric circuit.

Let c_i $(i = 1, 2, 3)$ be the concentrations of Na^+, K^+ and Cl^-, with valences $z_1 = z_2 = 1, z_3 = -1$. The PNP equations for the electric potential ψ and concentrations c_i are (Rubinstein, 1990; Song et al., 2018b)

$$\begin{aligned} &-\epsilon_0\epsilon_r\partial_{xx}\psi = e_0N_A\left(\sum_i z_ic_i + q\right), \quad x \in (0,a)\cup(a,b)\cup(b,L),\\ &\partial_t c_i = -\partial_x J_i, \quad J_i = -D_i\left(\partial_x c_i + \frac{z_ie_0}{k_BT}c_i\partial_x\psi\right), \quad i = 1,2,3, \end{aligned} \tag{3}$$

where q is the fixed permanent charge which is nonzero in the IC space (a, b), L is the typical length of electrocyte, J_i are the ionic fluxes consisting of two parts due to the ionic concentration gradient and the electric field, and D_i are the diffusion constants. Other parameters (see Appendix C) include vacuum permittivity ϵ_0, relative permittivity ϵ_r, elementary charge e_0, Avogadro constant N_A, Boltzmann constant k_B, and absolute temperature T.

Various currents can go through the two membranes (Hille et al., 2001; Hodgkin and Huxley, 1990; Xu and Lavan, 2008; Cao et al., 2019; Adams, 1981; Bezanilla, 2007). On the innervated membrane at $x = a$, there are voltage-gated channels, inward rectifier K^+ (Kir) channels, and acetylcholine receptors (AChRs). The currents I_i^{VG} $(i = 1, 2, 3)$ through voltage-gated channels involve the gating variables, whose dynamics depends on the membrane potential V_m^a. They are mainly responsible for the generation of AP. The Kir channels provide additional current for K^+, denoted by I_2^{Kir}. The receptors will be open based on a chemical binding process, and provide the stimulus currents I_i^R $(i = 1, 2)$ that are necessary to disturb the equilibrium state and trigger AP. On the non-innervated membrane at $x = b$, there are both channels (not voltage-gated) and pumps, with currents I_i^b and I_i^{pump} (i=1,2,3). The pumps are responsible to maintain and recover the equilibrium state for concentrations and electric potential. The general forms of the formulas of various currents have been discussed in a previous work Cao et al. (2019), and are not repeated here. Specific models for these currents are adopted in this paper and given in Appendix A.

These currents across the two membranes provide the flux conditions at $x = a, b$ for the PNP system

$$\begin{aligned} -z_1e_0N_AJ_1 &= I_1^{VG} + I_1^R, \quad \text{at} \quad x = a,\\ -z_2e_0N_AJ_2 &= I_2^{VG} + I_1^R + I_2^{Kir}, \quad \text{at} \quad x = a,\\ -z_3e_0N_AJ_3 &= I_3^{VG}, \quad \text{at} \quad x = a,\\ z_ie_0N_AJ_i &= I_i^b + I_i^{pump}, \quad i = 1,2,3 \quad \text{at} \quad x = b. \end{aligned} \tag{4}$$

We assume that the electric field is constant in the membranes, which was also used to derive the Goldman-Hodgkin-Katz (GHK) model in the literature Hille et al. (2001). Then, by continuity of electric field, the interface conditions for ψ are

$$\epsilon_r\partial_x\psi(a,t) = \epsilon_r^m\frac{\psi_+^a - \psi_-^a}{h_m}, \quad \epsilon_r\partial_x\psi(b,t) = \epsilon_r^m\frac{\psi_+^b - \psi_-^b}{h_m}, \tag{5}$$

where h_m is the thickness of the membrane and ϵ_r^m is the relative permittivity of membrane. Hereafter, superscripts a, b denote the membranes at $x = a, b$, and subscripts $\pm$ denote the right and left limits of quantities on the membrane.

The electrocyte is connected to a resistor to form a circuit. Since the time scale is quite small, we use the Maxwell's equations to model the total current I_r in the resistor (Eisenberg et al., 2018)

$$\partial_x I_r = 0, \quad I_r = J_r + \epsilon_0\partial_t E, \quad E(x,t) = -\partial_x\psi, \tag{6}$$

where J_r includes all fluxes of charge with mass, including the dielectric properties of matter. Suppose the resistor has a conductivity σ and a dielectric constant ϵ_r^* (to distinguish with ϵ_r in PNP system), then we have

$$J_r = \sigma E + (\epsilon_r^* - 1)\epsilon_0\partial_t E. \tag{7}$$

By (6) and (7), we get

$$\partial_x I_r = 0, \quad I_r = \sigma E + \epsilon_0\epsilon_r^*\partial_t E, \quad E(x,t) = -\partial_x\psi, \quad L < x < L + L_r, \tag{8}$$

where the effective length of the small-scale resistor is denoted by L_r.

At the junction $x = L$, the electric potential and the total current are continuous

$$\psi(L+,t) = \psi(L-,t), \quad I_r(L+,t) = I_{pnp}(L-,t), \tag{9}$$

where the total current I_{pnp} in the PNP system will be defined in Section 2.4 (see (28)). For a closed circuit, the point $x = L_r + L$ is connected to the point $x = 0$. At the two ends $x = 0, L + L_r$, without loss of generality, we set

$$\psi(0,t) = \psi(L + L_r, t) = 0, \tag{10}$$

since in a circuit one point for the electric potential has to be fixed to ensure a unique solution of ψ. As a consequence of $(9)_2$, it will be proved later that the total current is automatically continuous at $x = 0$. Since the ions only appear in the electrocyte $(0 < x < L)$ and can not penetrate into the resistor, the boundary conditions for c_i are

$$J_i = 0, \quad i = 1,2,3, \quad \text{at} \quad x = 0, L. \tag{11}$$

For initial conditions, we adopt the typical bulk concentrations (Gotter et al., 1998),

$$\begin{aligned} c_1(x,0) &= 160\,\text{mM}, \quad c_2(x,0) = 2.5\,\text{mM},\\ c_3(x,0) &= 162.5\,\text{mM}, \quad \text{for} \quad 0 < x < a \text{ and } b < x < L,\\ c_1(x,0) &= 8.928\,\text{mM}, \quad c_2(x,0) = 72.048\,\text{mM},\\ c_3(x,0) &= 9.328\,\text{mM}, \quad \text{for} \quad a < x < b. \end{aligned} \tag{12}$$

Together with $q = -71.648$ mM in $a < x < b$, the above initial values satisfy the electro-neutrality condition. The initial condition for ψ is

$$\psi(x,0) = 0, \quad x \in (0, 1+L_r). \tag{13}$$

The above initial conditions are only used to generate the resting state for the electric potential and the concentrations before simulating the electric discharge.

2.3. Non-dimensionalisation

In this subsection, we present the dimensionless system, which will be the starting point for analysis and simulations in later sections. We adopt the scalings

$$\begin{aligned}
&\tilde{\psi} = \frac{\psi}{k_BT/e_0}, \quad \tilde{c}_i = \frac{c_i}{c_0}, \quad \tilde{q} = \frac{q}{c_0}, \quad \tilde{D}_i = \frac{D_i}{D_0}, \quad \tilde{t} = \frac{t}{L^2/D_0},\\
&\tilde{x} = \frac{x}{L}, \quad \tilde{h}_m = \frac{h_m}{L}, \quad \tilde{a} = \frac{a}{L}, \quad \tilde{b} = \frac{b}{L}, \quad \tilde{L}_r = \frac{L_r}{L}, \quad \tilde{J}_i = \frac{J_i}{D_0c_0/L},\\
&\tilde{\epsilon}_r^* = \frac{\epsilon_r^*}{\epsilon_r}, \quad \tilde{I}_r = \frac{I_r}{I_0}, \quad \tilde{\sigma} = \frac{\sigma}{\sigma_0},
\end{aligned} \tag{14}$$

where

$$I_0 = \frac{D_0c_0e_0N_A}{L}, \quad \sigma_0 = \frac{D_0c_0e_0^2N_A}{k_BT}. \tag{15}$$

All the currents on the right-hand side of (4) are also scaled by I_0. The associated conductances and permeabilities in the formulas of currents (see Appendix A) are scaled by

$$G_0 = \frac{c_0D_0e_0^2N_A}{k_BTL}, \quad P_0 = \frac{D_0}{L}. \tag{16}$$

The typical values are given in Appendix C.

In the following the tilde will be dropped and the same notations will be used to denote the dimensionless quantities. The dimensionless equations are given by

$$\begin{aligned}
-\epsilon^2\partial_{xx}\psi &= \sum_{k=1}^{3} z_kc_k + q, \quad x \in (0,a)\cup(a,b)\cup(b,1),\\
\partial_t c_i &= -\partial_x J_i = D_i\partial_x(\partial_x c_i + z_ic_i\partial_x\psi),\\
&\qquad x \in (0,a)\cup(a,b)\cup(b,1),\\
\partial_x I_r &= -\partial_x(\sigma\partial_x\psi + \epsilon^2\epsilon_r^*\partial_{tx}\psi) = 0, \quad x \in (1, 1+L_r),
\end{aligned} \tag{17}$$

where $i = 1,2,3$, $q = -0.4478$ in the IC space $(a,\ b)$, and $q = 0$ in other intervals. The parameter σ is the dimensionless conductance of the external resistor, and $\sigma \in [0,5]$ is adopted in the simulations of this work, where $\sigma = 0$ represents an insulator. The small dimensionless parameters ϵ in (17) and ϵ_m in the following (20) are defined by

$$\epsilon = \sqrt{\frac{\epsilon_0\epsilon_rk_BT}{e_0^2N_Ac_0L^2}} \approx 8.4\times10^{-6}, \quad \epsilon_m = \sqrt{\frac{\epsilon_0\epsilon_r^mk_BT}{e_0^2N_Ac_0L^2}} \approx 1.3\times10^{-6}. \tag{18}$$

At the membranes, the flux conditions are

$$\begin{aligned}
-z_1J_1 &= I_1^{VG} + I_1^R, \quad \text{at} \quad x = a,\\
-z_2J_2 &= I_2^{VG} + I_2^R + I_2^{Kir}, \quad \text{at} \quad x = a,\\
-z_3J_3 &= I_3^{VG}, \quad \text{at} \quad x = a,\\
z_iJ_i &= I_i^b + I_i^{pump}, \quad i = 1,2,3, \quad \text{at} \quad x = b.
\end{aligned} \tag{19}$$

All the dimensionless formulas for above currents are given in Appendix A and all other dimensionless values in this subsection are given in Appendix C. The interface conditions for ψ at two membranes become

$$\epsilon^2\partial_x\psi(a,t) = \frac{\epsilon_m^2}{h_m}(\psi_+^a - \psi_-^a), \quad \epsilon^2\partial_x\psi(b,t) = \frac{\epsilon_m^2}{h_m}(\psi_+^b - \psi_-^b). \tag{20}$$

With the definitions for dimensionless membrane potentials and membrane capacitance C_m (scaled by $e_0^2N_Ac_0L/k_BT$)

$$V_m^a = \psi_+^a - \psi_-^a, \quad V_m^b = \psi_-^b - \psi_+^b, \quad C_m = \frac{\epsilon_m^2}{h_m} \approx 4.5\times10^{-8}, \tag{21}$$

the two conditions in (20) can be written as

$$\epsilon^2\partial_x\psi(a,t) = C_mV_m^a, \quad \epsilon^2\partial_x\psi(b,t) = -C_mV_m^b. \tag{22}$$

At the junction $x = 1$ of electrocyte and resistor, the continuity conditions are

$$\psi(1+,t) = \psi(1-,t), \quad I_r(1+,t) = I_{pnp}(1-,t), \tag{23}$$

where I_{pnp} is defined in (28) and an explicit form for the second condition is given by (32). The boundary conditions for ψ are

$$\psi(0,t) = \psi(1+L_r,t) = 0. \tag{24}$$

The boundary conditions for c_i are

$$J_i(x,t) = 0, \quad i = 1,2,3, \quad \text{at} \quad x = 0,1. \tag{25}$$

The dimensionless initial conditions at $t = 0$ are given by

$$\begin{aligned}
c_1(x,0) &= 1, \quad c_2(x,0) = 0.0156, \quad c_3(x,0) = 1.0156,\\
&\qquad x \in (0,a)\cup(b,1),\\
c_1(x,0) &= 0.0558, \quad c_2(x,0) = 0.4503, \quad c_3(x,0) = 0.0583,\\
&\qquad x \in (a,b),
\end{aligned} \tag{26}$$

and

$$\psi(x,0) = 0, \quad x \in (0,1+L_r). \tag{27}$$

2.4. The total current

We define the total current for PNP system in the electrocyte as

$$I_{pnp} = \epsilon^2\partial_tE + \sum_{i=1}^{3} z_iJ_i = -\epsilon^2\partial_{tx}\psi - \sum_{i=1}^{3} z_iD_i(\partial_xc_i + z_ic_i\partial_x\psi), \tag{28}$$

which consists of the ionic fluxes and the induced current due to change of electric field (similar to the Maxwell's model for resistor). Taking the time derivative of $(17)_1$ and utilizing $(17)_2$, we get

$$\begin{aligned}
-\epsilon^2\partial_{txx}\psi &= \sum_{i=1}^{3} z_iD_i\partial_x(\partial_xc_i + z_ic_i\partial_x\psi),\\
\Leftrightarrow \quad \partial_xI_{pnp} &= 0, \quad x \in (0,a)\cup(a,b)\cup(b,1).
\end{aligned} \tag{29}$$

This implies that the total current I_{pnp} in the PNP system is a constant in space (i.e., IC and EC spaces) or is a function of time only. Since all fluxes J_i $(i = 1,2,3)$ and the electric field $E = -\partial_x\psi$ are continuous at membranes $x = a, b$, so is the total current I_{pnp} by (28). Then, by (29), the total current is uniform in the electrocyte

$$I_{pnp}(x,t) = I^*(t), \quad 0 < x < 1. \tag{30}$$

By $(17)_3$ the total current I_r in the resistor is a constant in space. Since the total current is continuous at the junction $x = 1$ between the electrocyte and the resistor, the total current for the whole system is spatially uniform

$$I_{pnp}(x,t) = I_r(x,t) = I^*(t), \quad 0 \le x \le 1+L_r. \tag{31}$$

This is expected in a closed circuit, and justifies the above definition of I_{pnp}. As in Maxwell's model for resistor, the induced current

$\epsilon^2\partial_t E$ is important and should be retained in the definition of the total current for the PNP system. Eq. (31) implies that the continuity of the total current at $x = 0$ (or $x = 1 + L_r$) automatically holds.

With the definition in (28) and zero flux conditions in (25), the continuity of the total current in $(23)_2$ is explicitly given by

$$\epsilon^2\partial_{tx}\psi(1-,t) = \epsilon^2\epsilon_r^*\partial_{tx}\psi(1+,t) + \sigma\partial_x\psi(1+,t). \tag{32}$$

As there is no ionic flux to the resistor, the nonzero total current $I^*(t)$ is passed from the electrocyte to the resistor through the term $\epsilon^2\partial_{tx}\psi$ in I_{pnp} at $x = 1$. This indicates a possible BL near $x = 1$, where $\partial_x\psi$ is large.

Suppose $I^*(t)$ is a given parameter or function, the Eq. (17) in the resistor becomes

$$I_r(x,t) = \sigma E + \epsilon^2\epsilon_r\partial_t E = I^*(t), \quad 1 < x < 1 + L_r. \tag{33}$$

where $E = -\partial_x\psi$. Then, with the conditions

$$\begin{aligned} E(x,0) &= 0, \quad 1 < x < 1 + L_r \\ \psi(1 + L_r, t) &= 0, \quad t > 0, \end{aligned} \tag{34}$$

we get the solutions for the resistor system

$$\begin{aligned} E(x,t) &= E^*(t) = \int_0^t \frac{I^*(s)}{\epsilon^2\epsilon_r} e^{\sigma(s-t)/\epsilon^2\epsilon_r} ds, \\ \psi(x,t) &= E^*(t)(1 + L_r - x). \end{aligned} \tag{35}$$

Depending on the relative scale of σ and ϵ, approximation of the above integral or Eq. (33) is possible. The continuity of ψ at $x = 1$ then provides

$$\psi(1,t) = E^*(t)L_r. \tag{36}$$

The above condition can be considered as an effective boundary condition for the PNP system to replace the resistor. In general, this condition depends on history of the total current $I^*(t)$, which is related with the PNP system.

3. Asymptotic analysis and ODE model

Two dimensionless parameters ϵ and σ play important roles in the previous formulation. It is well known that there are BLs and accumulation of ions on the two sides of membranes at $x = a, b$, due to the small parameter ϵ. Depending on the scale of σ, there could also be BLs at the junctions $x = 0, 1$ due to the change of forms of currents from the electrocyte to the resistor. In this section, asymptotic analysis is conducted to derive a leading order ODE model from the PNP+resistor model.

There have been a number of BL analyses near membranes for the PNP system (see Song et al. (2018b); Cao et al. (2019), which show BLs of thickness $O(\epsilon)$ on two sides of membranes under normal physiological conditions. Hereafter, we use "bulk" to mean the bulk/inner region away from the BLs near membranes or the junctions between electrocyte and resistor. In bulk regions, all the concerned quantities are at most $O(1)$ and taking the spacial derivative ∂_x will not increase the order since there is no internal layer in bulk. In other words, we have

$$\begin{aligned} &\psi, \partial_x\psi, \ldots = O(1), \quad c_i, \partial_x c_i, \ldots = O(1), \quad J_i, \partial_x J_i, \ldots = O(1), \\ &i = 1, 2, 3. \end{aligned} \tag{37}$$

From experiments in the literature and simulations in the next section, the relevant time scale for the AP generation and electric discharge is milliseconds (see also the parameter α_0 in (A.5,C.2)). It is much smaller than diffusion time scale (at the order of 10 s), by an order of roughly $O(\epsilon)$. Therefore, as in a previous work Cao et al. (2019), we adopt a new time scale $\hat{t} = t/\epsilon$ in the following analysis and $\hat{t} \sim O(1)$ is the order of interest. The asymptotic analysis here is then slightly different from the classical one with the diffusion time scale. From (17) we get

$$\begin{aligned} -\epsilon^2\partial_{xx}\psi &= \sum_{k=1}^{3} z_k c_k + q, \quad x \in (0,a) \cup (a,b) \cup (b,1), \\ \partial_{\hat{t}} c_i &= -\epsilon\partial_x J_i = \epsilon D_i\partial_x(\partial_x c_i + z_i c_i\partial_x\psi), \\ &\quad x \in (0,a) \cup (a,b) \cup (b,1), \\ &\quad \partial_x(\sigma\partial_x\psi + \epsilon\epsilon_r^*\partial_{\hat{t}x}\psi) = 0, \quad 1 < x < 1 + L_r, \end{aligned} \tag{38}$$

where $i = 1, 2, 3$.

The second equation $(38)_2$ implies that the temporal variation of c_i in bulk is $O(\epsilon)$, and then each concentration c_i remains as the initial constant in bulk at leading order. Taking the derivative ∂_x on $(38)_2$ gives

$$\partial_{\hat{t}}(\partial_x c_i) = -\epsilon\partial_{xx} J_i = O(\epsilon), \quad i = 1, 2, 3. \tag{39}$$

By initial conditions, we have $\partial_x c_i = 0$ at $\hat{t} = 0$ and hence $\partial_x c_i = O(\epsilon)$ for any $\hat{t} \sim O(1)$ in bulk. As a result, the fluxes are dominated by the drift term due to the electric field

$$\begin{aligned} &J_i = -D_i(\partial_x c_i + z_i c_i\partial_x\psi) = -D_i z_i c_i\partial_x\psi + O(\epsilon), \\ &i = 1, 2, 3, \text{ in bulk.} \end{aligned} \tag{40}$$

Similarly by (28), together with (40), the total current in PNP is written as

$$\begin{aligned} I_{pnp} &= -\epsilon\partial_{\hat{t}x}\psi + \sum_{i=1}^{3} z_i J_i \\ &= -\sum_{i=1}^{3} D_i z_i^2 c_i\partial_x\psi + O(\epsilon), \quad \text{in bulk,} \end{aligned} \tag{41}$$

where $\sum_{i=1}^{3} D_i z_i^2 c_i$ can be interpreted as an effective conductance for PNP system (compared with σ in Maxwell model (8) for resistor). Near the junctions $x = 0, 1$, the term $\epsilon\partial_{\hat{t}x}\psi$ in the total current I_{pnp} in (41) becomes significant. Since the ionic fluxes are zero at two ends of the electrocyte by (25), we obtain from (41) that

$$I_{pnp} = -\epsilon\partial_{\hat{t}x}\psi, \quad \text{at} \quad x = 0, 1. \tag{42}$$

Initially, $\partial_x\psi = 0$, and there is no current and no BLs at $x = 0, 1$. But during dynamics with nonzero total current, the quantity $\partial_{\hat{t}x}\psi$ becomes significant near $x = 0, 1$, leading to large $\partial_x\psi$ and BLs. In BL, the large $\partial_x\psi$ will be balanced by $\partial_x c_i$, by noting $J_i = 0$ at $x = 0, 1$. Across the BL from the bulk to the junctions $x = 0, 1$, the major contribution of I_{pnp} changes from ionic fluxes in (41) to the term $\epsilon\partial_{\hat{t}x}\psi$ in (42).

Suppose the maximum scale of the total current is $O(\delta)$, i.e.,

$$I_{pnp} = I_r = I^*(\hat{t}) \sim O(\delta). \tag{43}$$

By (41), we can also consider δ as the maximum scale of $\partial_x\psi$ in bulk regions of electrocyte during the dynamic process. By the definition of total current I_r in resistor, we may interpret δ as $\delta = \max\{\epsilon, \sigma\}$, and we assume

$$O(\epsilon) \le O(\delta) \le O(1). \tag{44}$$

Based on estimates of previous work on the open circuit Cao et al. (2019), the individual fluxes across membranes are $\le O(1)$ (e.g., the fluxes are $\sim 0.01 - 0.1$ in Fig. 7 therein), so this assumption in (44) is consistent with the scale of membrane currents. In BLs near $x = 0, 1$, the variation of ψ is also estimated as $O(\delta)$.

In the following, we set $\epsilon_r^* = O(1), L_r = O(1)$ and treat ϵ as a fixed small parameter. Then the problem depends on the scale of σ, leading to different cases as in the next subsections.

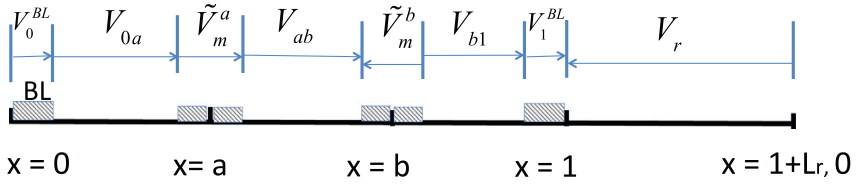

Fig. 3. The BLs and differences in electric potential.

3.1. Open circuit

The case of open circuit in Cao et al. (2019) can be recovered with

$$\sigma \le O(\epsilon), \tag{45}$$

which is a resistor with large resistance (or approximately an insulator).

We take the junction $x = 1$ for illustration. By the definition (28) and the condition (32) at $x = 1$, in the new time scale we get

$$-I^*(\hat{t}) = \epsilon \partial_{\hat{t}x}\psi(1-,\hat{t}) = \epsilon\epsilon_r^* \partial_{\hat{t}x}\psi(1+,\hat{t}) + \sigma\partial_x\psi(1+,\hat{t}). \tag{46}$$

By (35), the electric field is spatially uniform in resistor, and we have

$$\partial_x\psi(1+,\hat{t}) = \frac{\psi(1+L_r,\hat{t}) - \psi(1+,\hat{t})}{L_r} = -\frac{\psi(1+,\hat{t})}{L_r} = O(1). \tag{47}$$

Substituting (47,45) into (46) leads to

$$-I^* = \epsilon\partial_{\hat{t}x}\psi(1-,\hat{t}) = O(\epsilon) + O(\sigma) = O(\epsilon), \tag{48}$$

which implies $\delta = \epsilon$ in (44). Therefore the total current is negligibly small, as in the open circuit case.

For the open circuit case in Cao et al. (2019), the boundary condition $\partial_x\psi = 0$ at $x = 1$ was imposed as an ideal case from the perspective of symmetry in the middle of EC space. When the electrocyte is connected to a resistor (or an insulator), this is not exactly true, and the above estimate (48) and Eq. (46) imply $\partial_x\psi(1-,\hat{t}) = O(1)$. However, we have two observations. First, there is a tiny BL near the junction $x = 1$, where the variation of ψ is small at order $O(\epsilon)$ since the thickness of BL is $O(\epsilon)$. As a result, the variation or BL near $x = 1$ can be neglected. Second, in the bulk region just away from the BL near $x = 1$, we get

$$\partial_x\psi = O(I^*) = O(\epsilon). \tag{49}$$

Essentially, we have $\partial_x\psi = 0$ or constant ψ in bulk, which is the typical feature in the open circuit case.

3.2. Closed circuit with finite total current

In the situation when the electric eel attacks the prey, the equivalent mini-resistor has a conductance much larger than $O(\epsilon)$. We consider the case of a common closed circuit with

$$\epsilon \ll \sigma \le O(1), \tag{50}$$

which will induce finite current of $O(\delta) \sim O(\sigma)$ in (44). The BLs and differences in electric potential (voltage) are illustrated in Fig. 3. Unlike the open circuit case, the variation V_1^{BL} in BL near $x = 1$ is not negligible, as the total current is no longer small. The voltage drops will be studied one by one.

First, in the resistor, by (46) at leading order, we get

$$-I^*(\hat{t}) = \sigma\partial_x\psi(1+,\hat{t}). \tag{51}$$

Then, by the uniform electric field in (35) for the resistor system, we get

$$V_r = \psi(1,\hat{t}) - \psi(1+L_r,\hat{t}) = \frac{L_r}{\sigma}I^*(\hat{t}). \tag{52}$$

which can also be derived from (35,36) as leading approximation.

Second, we consider the voltage drops in bulk regions. Since it is shown below (38) that the variation of c_i is $O(\epsilon)$, we treat the concentrations in bulk as constants, denoted by c_{iI} and c_{iE} $(i = 1, 2, 3)$ for the IC and EC spaces. Then we define the two effective conductances as

$$\sigma_I = \sum_{i=1}^{3} D_i z_i^2 c_{iI} \quad x \in (a,b),$$
$$\sigma_E = \sum_{i=1}^{3} D_i z_i^2 c_{iE} \quad x \in (0,a)\cup(b,1). \tag{53}$$

Together with (41,43), we get

$$-\sigma_I\partial_x\psi = I^*, \quad x \in (a,b), \tag{54}$$

which gives difference in electric potential from a to b

$$V_{ab} := \psi_L^b - \psi_R^a = \frac{a-b}{\sigma_I}I^*, \tag{55}$$

where and hereafter subscripts L, R denote the left-side and right-side limits of bulk quantities (not in BL). Similarly, we have

$$V_{0a} := \psi_L^a - \psi_R^0 = -\frac{a}{\sigma_E}I^*, \quad V_{b1} := \psi_L^1 - \psi_R^b = \frac{b-1}{\sigma_E}I^*. \tag{56}$$

Next, we examine the membrane potentials at $x = a, b$. By definition (28) in the new time scale $\hat{t}$ and with (43), we have

$$-\epsilon\partial_{\hat{t}x}\psi + \sum_{i=1}^{3} z_i J_i = I^*(\hat{t}). \tag{57}$$

Then at $x = a, b$ and by using (19,22), we get

$$-\frac{C_m}{\epsilon}\partial_{\hat{t}}V_m^a = I_1^{VG} + I_2^{VG} + I_3^{VG} + I_1^R + I_2^R + I_2^{Kir} + I^*$$
$$\frac{C_m}{\epsilon}\partial_{\hat{t}}V_m^b = -\sum_{i=1}^{3}(I_i^b + I_i^{pump}) + I^*. \tag{58}$$

The factor $1/\epsilon$ appears because we adopted a new time scale. It is estimated by BL analysis in Song et al. (2018b); Cao et al. (2019) that the variation of ψ in BLs near membranes is small. In deriving the above equation (58) including the definition of the total current I^* in Section 2.4, no approximation (like electro-neutrality condition) is made, in other words it is exact and derived from the PNP system.

As first approximation, we can replace the membrane potentials by

$$V_m^a \approx \tilde{V}_m^a = \psi_R^a - \psi_L^a, \quad V_m^b \approx \tilde{V}_m^b = \psi_L^b - \psi_R^b. \tag{59}$$

By keeping high-order terms, a more accurate approximation is given by

$$V_m^a = \tilde{V}_m^a f_c, \quad V_m^b = \tilde{V}_m^b f_c$$
$$f_c = 1 - \frac{C_m}{\epsilon}\left(\frac{1}{\sqrt{c_{1I}+c_{2I}+c_{3I}}} + \frac{1}{\sqrt{2c_{3E}}}\right) + o(C_m/\epsilon), \tag{60}$$

where f_c is a fixed correction factor. The membrane currents in (58) involve membrane potentials and concentrations, given by formulas in Appendix A. In these formulas, we can use the bulk membrane potentials $\tilde{V}_m^a, \tilde{V}_m^b$ and bulk concentrations as first approximations. To be consistent with (60), similar high-order approximations for concentrations are

$$c^a_{i,-} = c_{iE}\left(1 - \frac{C_m}{\epsilon}\frac{z_i\tilde{V}_m^a}{\sqrt{2c_{3E}}}\right), \quad c^a_{i,+} = c_{iI}\left(1 + \frac{C_m}{\epsilon}\frac{z_i\tilde{V}_m^a}{\sqrt{c_{1I}+c_{2I}+c_{3I}}}\right),$$
$$c^b_{i,-} = c_{iI}\left(1 + \frac{C_m}{\epsilon}\frac{z_i\tilde{V}_m^b}{\sqrt{c_{1I}+c_{2I}+c_{3I}}}\right), \quad c^b_{i,+} = c_{iE}\left(1 - \frac{C_m}{\epsilon}\frac{z_i\tilde{V}_m^b}{\sqrt{2c_{3E}}}\right). \tag{61}$$

The derivation of 59–(61) is given in Appendix D.

Remark: For the formulas of currents I_i^{VG}, I_2^{Kir} and I_i^b in $(A.8)_{1,2,4}$, the $O(C_m/\epsilon)$ corrections in (60,61) cancel each other, therefore the first approximations with bulk values are as accurate as those with (60,61). This is consistent with the fact (Song et al., 2018a) that the electro-chemical potential is constant (with error $O(\epsilon) \ll O(C_m/\epsilon)$) across the BL. The formulas I_i^b in $(A.8)_3$ and I_1^R in (A.4, A.5) are slightly different with corrections in (60,61).

Finally we study the BLs at $x = 0, 1$ and the differences in electric potential V_0^{BL} and V_1^{BL}. For BL at $x = 1$, we get at leading order (see derivation in Appendix D)

$$\epsilon\,\partial_x\psi(1-,\hat{t}) = \sqrt{2c_{3E}}(e^{V_1^{BL}/2} - e^{-V_1^{BL}/2}), \tag{62}$$

where

$$V_1^{BL} = \psi_-^1 - \psi_L^1 = \psi(1-,\hat{t}) - \psi_L^1. \tag{63}$$

Using the total current (46) at $x = 1$, we obtain

$$\partial_{\hat{t}}\left[\sqrt{2c_{3E}}\left(e^{V_1^{BL}/2} - e^{-V_1^{BL}/2}\right)\right] = -I^*, \tag{64}$$

which is equivalent to

$$\left(e^{V_1^{BL}/2} + e^{-V_1^{BL}/2}\right)\sqrt{\frac{c_{3E}}{2}}\,\partial_{\hat{t}}V_1^{BL} = -I^*. \tag{65}$$

Similarly V_0^{BL} follows the same equation, and hence $V_0^{BL} = V_1^{BL}$.

Finally, by the closed circuit (see Fig. 3), we get the equation for I^*,

$$V_0^{BL} + V_{0a} + \tilde{V}_m^a + V_{ab} - \tilde{V}_m^b + V_{b1} + V_1^{BL} = V_r, \tag{66}$$

which, by substituting (52,55,56), leads to

$$\tilde{V}_m^a - \tilde{V}_m^b + 2V_1^{BL} = \left(\frac{L_r}{\sigma} + \frac{b-a}{\sigma_I} + \frac{1-(b-a)}{\sigma_E}\right)I^*. \tag{67}$$

3.3. The ODE model

We summarize the system from the preceding subsection, called ODE model here. Now we convert the time scale from $\hat{t}$ back to diffusion time scale t, and the ODE model reads

$$\begin{aligned}
-C_m f_c\frac{d}{dt}\tilde{V}_m^a &= I_1^{VG} + I_2^{VG} + I_3^{VG} + I_1^R + I_2^R + I_2^{Kir} + I^*\\
C_m f_c\frac{d}{dt}\tilde{V}_m^b &= -\sum_{i=1}^{3}(I_i^b + I_i^{pump}) + I^*,\\
C_{BL}\frac{d}{dt}V_1^{BL} &= -I^*,\\
\tilde{V}_m^a - \tilde{V}_m^b + 2V_1^{BL} &= \left(\frac{L_r}{\sigma} + \frac{b-a}{\sigma_I} + \frac{1-(b-a)}{\sigma_E}\right)I^*,
\end{aligned} \tag{68}$$

where σ_I, σ_E are given in (53), C_m is membrane capacitance and

$$C_{BL} = \epsilon\left(e^{V_1^{BL}/2} + e^{-V_1^{BL}/2}\right)\sqrt{\frac{c_{3E}}{2}} \tag{69}$$

is the "capacitance" of the BL near the junction $x = 1$. Note that the capacitance C_{BL} describes the effect of accumulation of ions near the junction, and unlike the membrane capacitance it is not a constant. The factor f_c is given in (60), and if we adopt the first approximation we get $f_c = 1$, which implies the bulk membrane potentials $\tilde{V}_m^a, \tilde{V}_m^b$ are considered the same as exact membrane potentials V_m^a, V_m^b.

Now we compared with the intuitive mini circuit model in Section 2.1. The specific forms of various currents in (68) for electrocyte are adopted to represent $I_{channel}$ in (1), and the resistance is $R = L_r/\sigma$ in this 1D case. There are only two differences: (1) the term V_1^{BL} is added to account for the difference of electric potential across BL near the junction of electrocyte and resistor, (2) the voltage drops in IC and EC spaces are added on the right-hand side of (68), where the terms $(b-a)/\sigma_I$ and $[1-(b-a)]/\sigma_E$ are interpreted as the internal resistances of the IC and EC spaces of electrocyte. We note that I^* is often interpreted as the total current and used as a bifurcation parameter in the literature (e.g., the HH model). Here, we have verified this physical interpretation of the total current by clearly defining the total current in the PNP system and the closed circuit.

Remark: For the ODE model of an open circuit, we set $I^* = 0$ and $\sigma = 0$, and remove the last two equations in (68). This recovers the model in Cao et al. (2019), and can be used to capture the high voltage generation $\tilde{V}_m^a - \tilde{V}_m^b$.

3.4. The macroscopic circuit model

We first present a formal analysis based on superposition principle, to get an idea of the connection between macroscopic circuit and the mini circuit. Then, we show the macroscopic circuit model based on the ODE model in (68).

The electric organ consists of thousands of electrocytes stacked in series. The stacked electrocytes can be considered as a series of battery, which provide the total macroscopic voltage V^{macro}. When it is connected to an external resistor with resistance R^{macro}, there will be current I^{macro} through the macroscopic circuit. If we envision it as a Kirchhoff circuit, we get

$$I^{macro} = \frac{V^{macro}}{R^{macro}}. \tag{70}$$

We use dimensional quantities in the formulation. Assume there are N electrocytes in the organ, then we write

$$V^{macro} = NV_{pnp} \approx N(\psi(L,t) - \psi(0,t)) = NV_r, \tag{71}$$

where ψ is from the PNP system for unit electrocyte structure. We assume a simple resistor of regular shape for simplicity, then the total resistance is

$$R^{macro} = \rho\frac{L_r^{macro}}{A_r}, \tag{72}$$

where $\rho = 1/\sigma$ is resistivity (considered as material property), L_r^{macro} is the length of resistor, and A_r is cross sectional (contact) area. Diving the total resistor into N parts of mini-resistors $L_r^{macro} = NL_r$, we can write

$$R^{macro} = NR, \quad R = \rho\frac{L_r}{A_r} = \frac{L_r}{\sigma A_r}, \tag{73}$$

where L_r is the length of mini resistor used in previous formulation. The macroscopic length scale of electric organ is expected to be the same order as that of the resistor (e.g., the prey or an arm), then we expect $L_r \sim O(L)$ as adopted in previous analysis. Combining (70,71,73), we get

$$I^{macro} \approx \frac{V_r}{R} = A_r\frac{V_r\sigma}{L_r} = A_rI^*(t), \tag{74}$$

where Eq. (52) is used in last equality. Therefore, the total current in the macroscopic circuit only differs from the previous I^* for mini

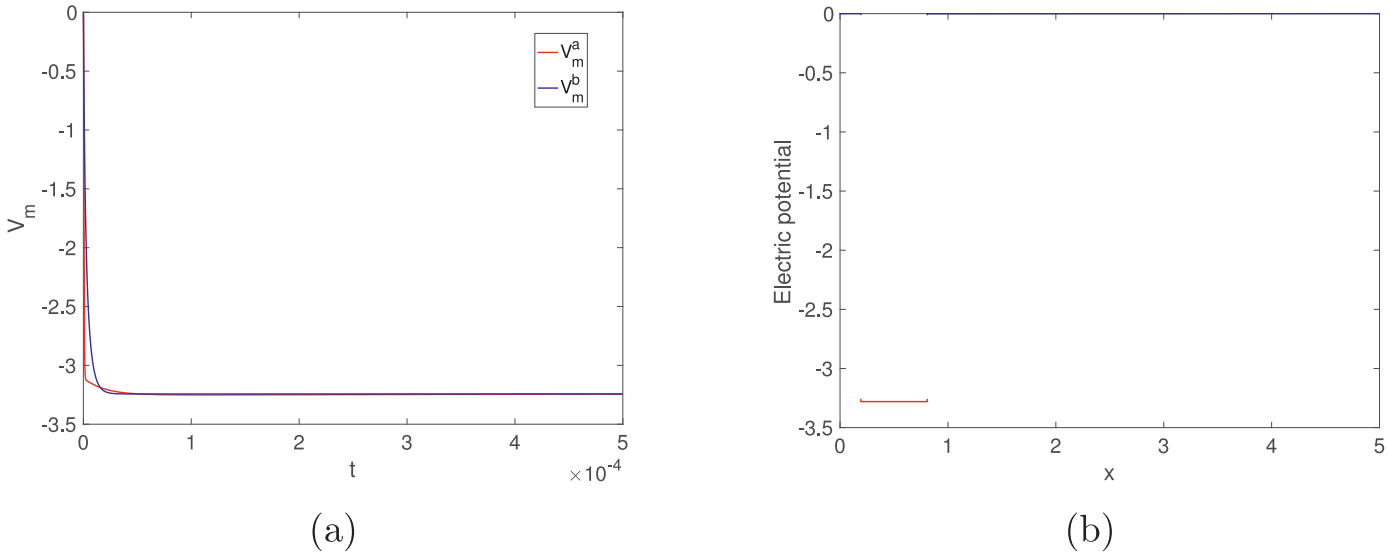

Fig. 4. Numerical results to generate the resting state in step 1; (a) the dynamics of membrane potential V_m (b) Distribution of electric potential at resting state.

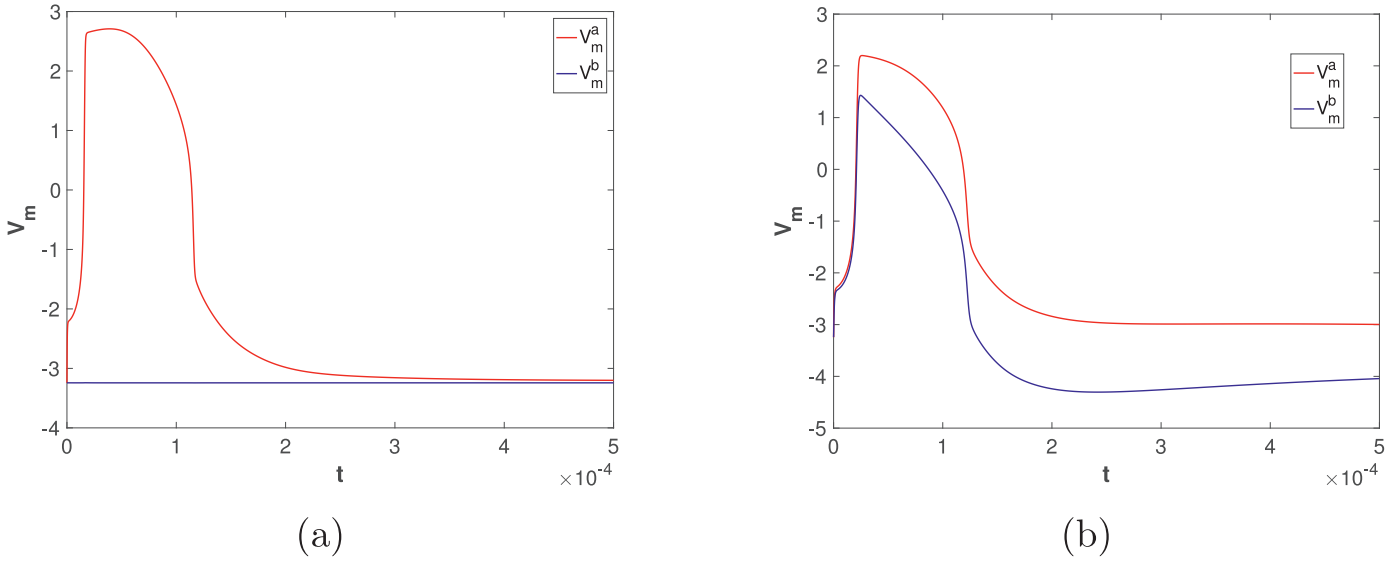

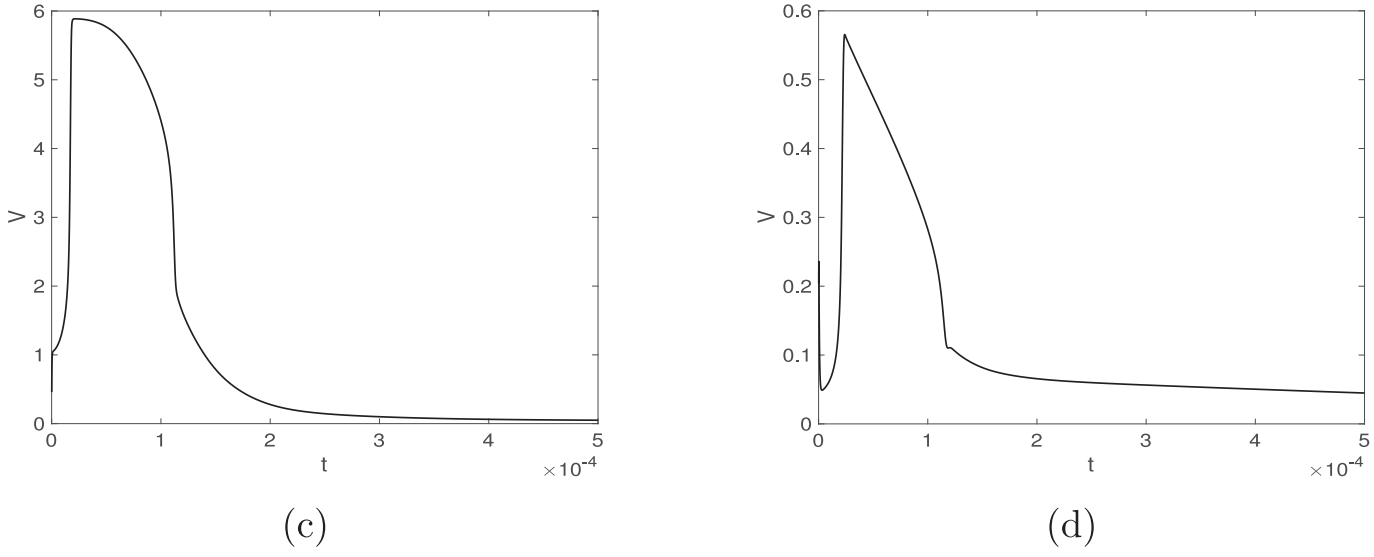

Fig. 5. The dynamics of membrane potentials: (a) $\sigma = 0$, (b) $\sigma = 1$; and voltage difference over the entire electrocyte: (c) $\sigma = 0$, (d) $\sigma = 1$.

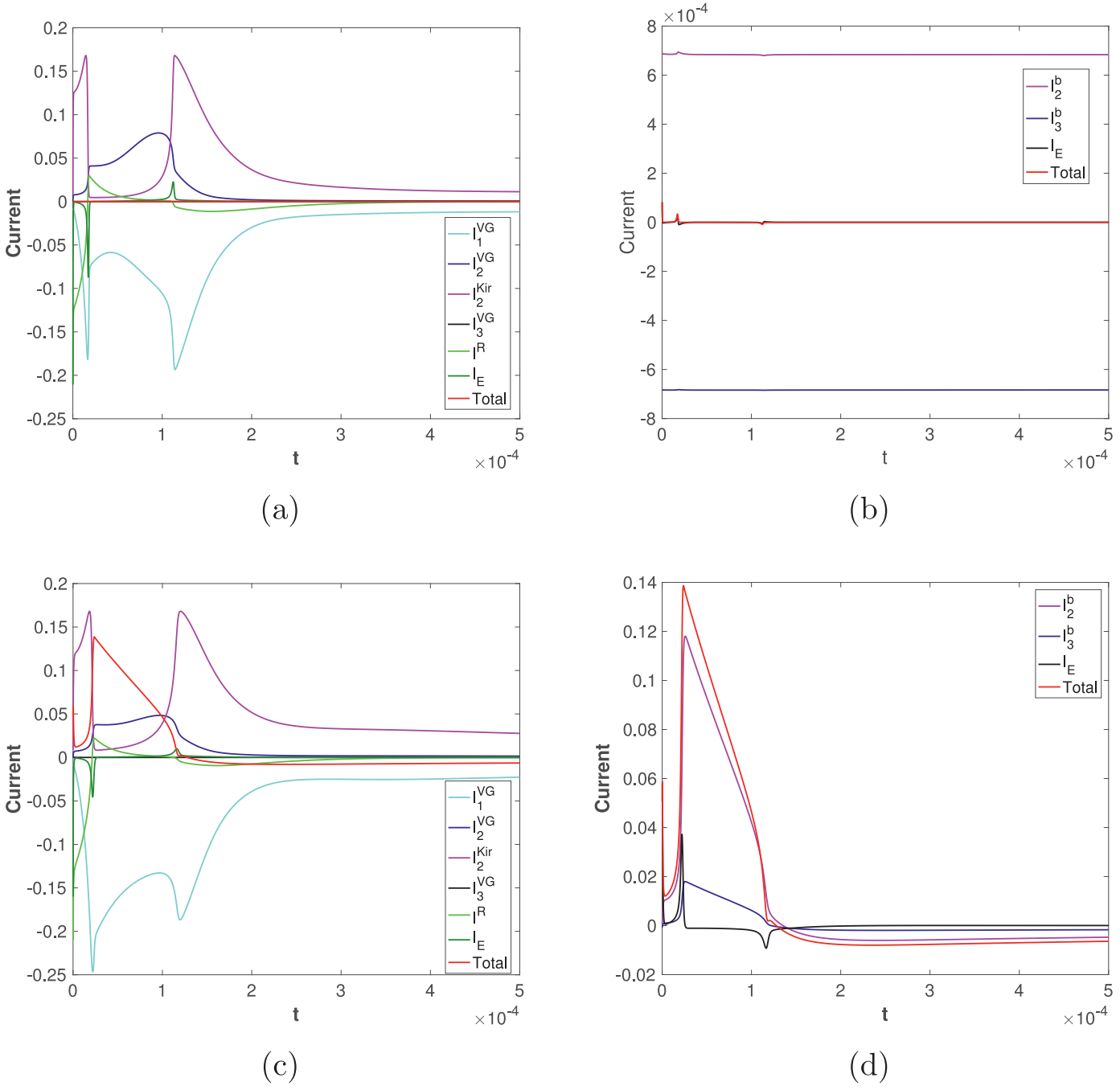

Fig. 6. The dynamics of various currents and the total current on the two membranes (a) the innervated membrane with $\sigma = 0$, (b) the non-innervated membrane with $\sigma = 0$, (c) the innervated membrane with $\sigma = 1$, (d) the non-innervated membrane with $\sigma = 1$, where I_E means the induced current $-\epsilon^2 \partial_{tx}\psi$.

circuit by a factor of contact area, which makes sense since a 1D formulation was adopted.

To examine more closely, we find that approximation in (71) is not so accurate, since the BLs at the junction between electrocyte and resistor are repeatedly counted. For stacked electrocytes, the connection between the electrocytes is different from the connection between electrocyte and resistor. There is no change of forms of currents, the conditions would be continuities of electric potential, concentrations, and fluxes, instead of the condition (9). There will be no BL at connection of electrocytes in EC space, and the two BLs related with V_0^{BL}, V_1^{BL} only appear at junctions at far end. Based on the previous ODE model, the last algebraic equation should be replaced by

$$N\tilde{V}_m^a - N\tilde{V}_m^b + 2V_1^{BL} = N\left(\frac{L_r}{\sigma} + \frac{b-a}{\sigma_I} + \frac{1-(b-a)}{\sigma_E}\right)I^*. \tag{75}$$

As $N \sim O(10^3)$, by dividing N, the above term V_1^{BL}/N or the effect of junction point is negligible. Now we summarize the macroscopic circuit model

$$-C_m f_c \frac{d}{dt}\tilde{V}_m^a = I_1^{VG} + I_2^{VG} + I_3^{VG} + I_1^R + I_2^R + I_2^{Kir} + I^*$$

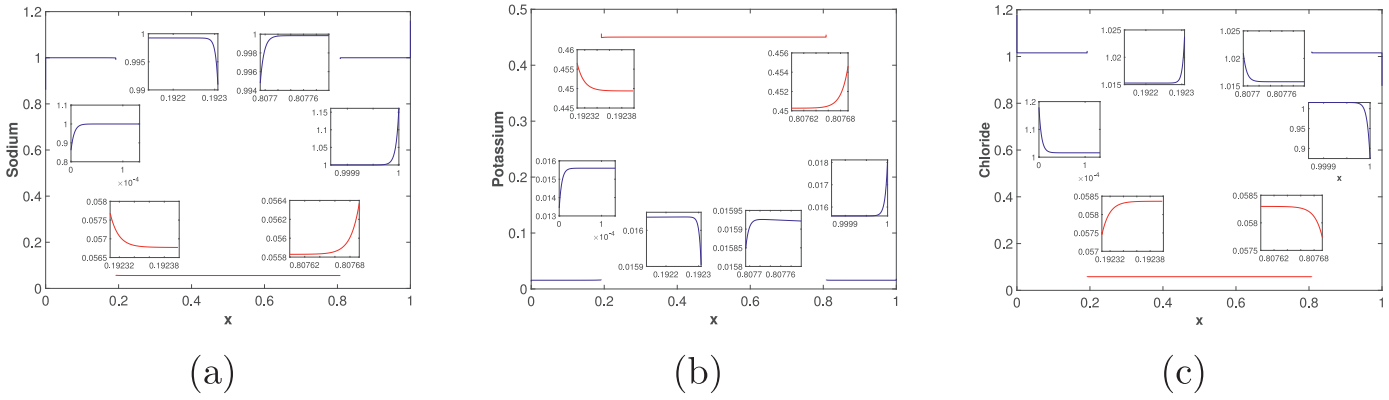

Fig. 7. The profiles of concentrations c_i $(i = 1, 2, 3)$ for sodium, potassium and chloride, at $t = 3 \times 10^{-5}$.

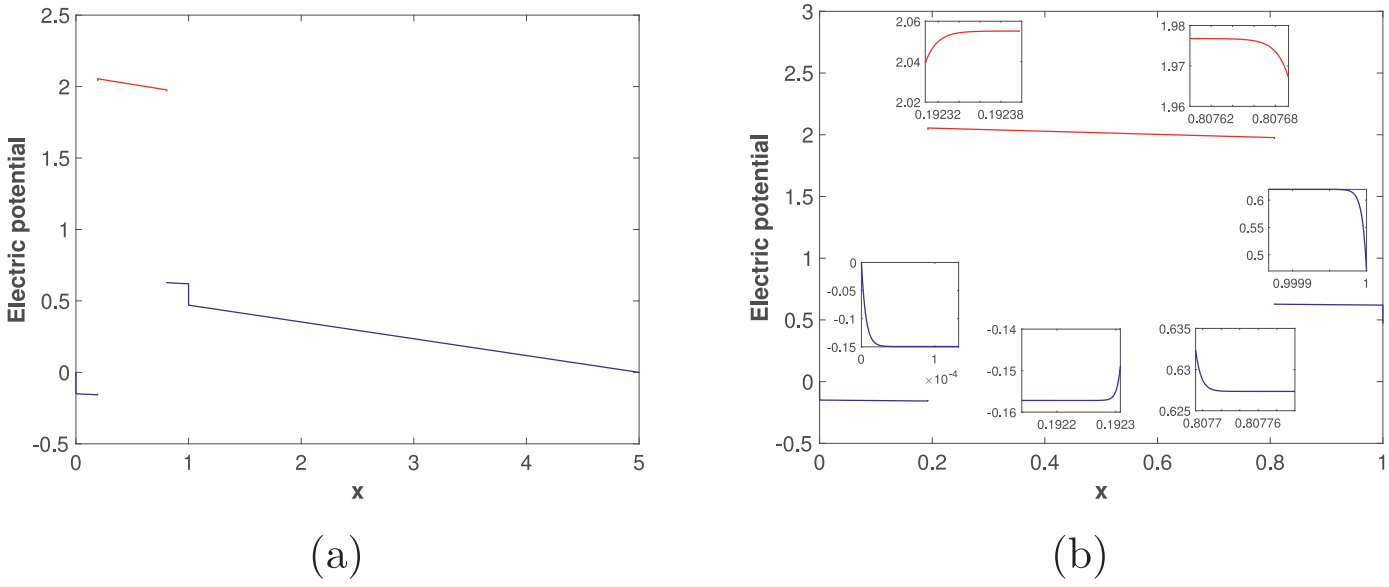

Fig. 8. The profile of the electric potential ψ at $t = 3 \times 10^{-5}$: (a) the whole region, (b) the region for PNP system and BLs.

$$C_m f_c \frac{d}{dt}\tilde{V}_m^b = -\sum_{i=1}^{3}(I_i^b + I_i^{pump}) + I^*,$$
$$\tilde{V}_m^a - \tilde{V}_m^b = \left(\frac{L_r}{\sigma} + \frac{b-a}{\sigma_I} + \frac{1-(b-a)}{\sigma_E}\right)I^*, \tag{76}$$

where the quantities C_m, f_c, σ_E, σ_I are the same as in (68) and the 3D total current is $I^{macro} = A_r I^*$ by (74).

This model justifies the circuit models in the literature. In early studies Bennett (1970, 1961), equivalent electric circuits with same structure as $(76)_3$ were adopted to study the electric organs and electrosensory systems. Also, recent experimental studies (Catania, 2017a; 2017b; 2016) adopted similar equivalent circuit as $(76)_3$ to study the electric discharge with leaping bahaviour of eels, where the electric organ is modelled as the electromotive force with internal resistance.

Here we emphasize the coupling of dynamics of membrane potentials $(76)_{1,2}$ with the circuit equation $(76)_3$. First, detailed terms for currents from various mechanisms are incorporated into the system, and the conductances in these currents and other parameters will play an important role in the magnitude and pattern of the total current, which are possibly related to different biological behaviors of eels. Second, some experimental works (Catania, 2017a; 2017b; 2016) often adopt the single circuit equation $(76)_3$ to illustrate the phenomenon. However, unlike the real battery that gives constant voltage, the electrocytes provide a dynamic voltage. As shown in later simulations, the maximum voltage during the dynamics varies a lot with different resistances of the external resistor. It means that we should distinguish the cases of insulator (maximum voltage reported) and conductor (maximum current reported) for the external resistor.

4. Numerical results

In this section, we present the numerical results of the PNP+resistor system and the ODE models. Comparison between the two models are made, and the features different from open circuit will be demonstrated. Then, we interpret the results to estimate the current for the macroscopic circuit.

4.1. PNP+Resistor model

In this subsection, we present numerical results for the dimensionless PNP+resistor model in Section 2.3. The formulas for the membrane currents in Appendix A are used, including I_i^b in $(A.8)_3$. We set $L_r = 4$ for illustration. We simulate it in two steps. First, we generate the resting (equilibrium) state for the electrocyte by setting $\sigma = 0$ and $I_1^R = I_1^* = 0$ in (19,A.4), when the receptors are closed. Second, we simulate the dynamic processes for both the

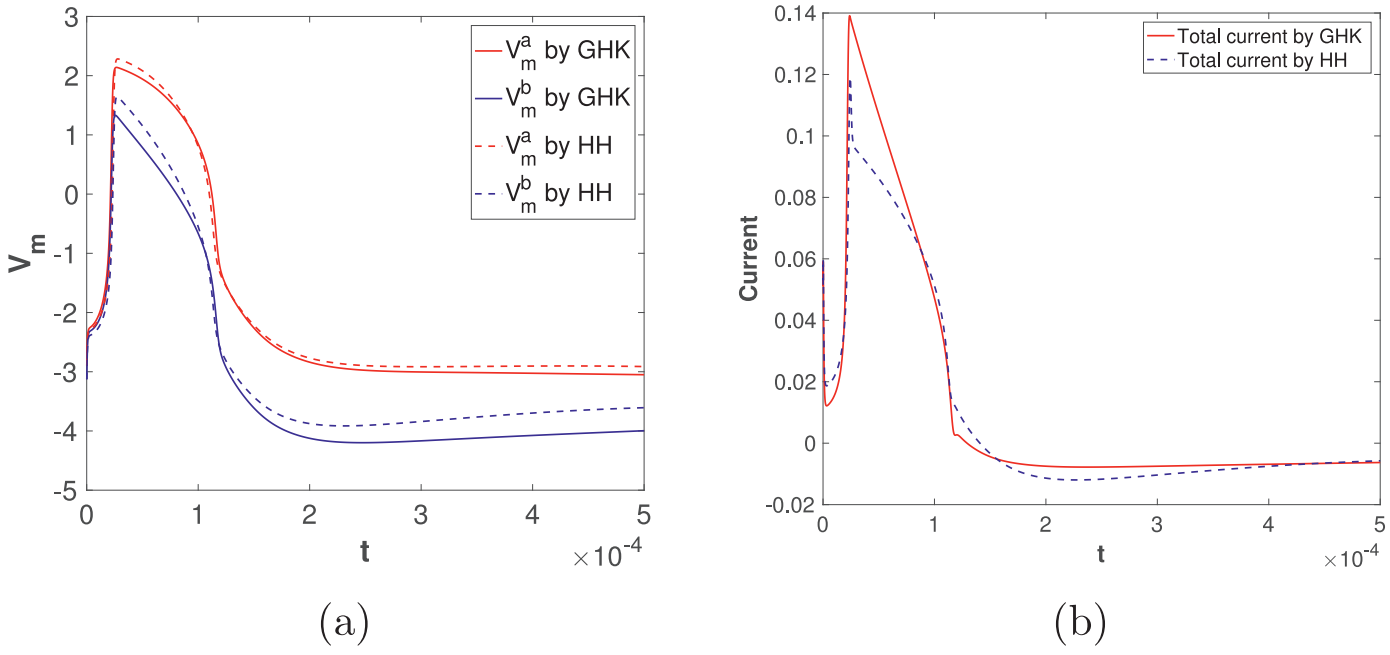

Fig. 9. Comparison of results with GHK and HH models of I_i^b in $(A.8)_3$ and $(A.8)_4$ for the case $\sigma = 1$: (a) membrane potentials, (b) the total current.

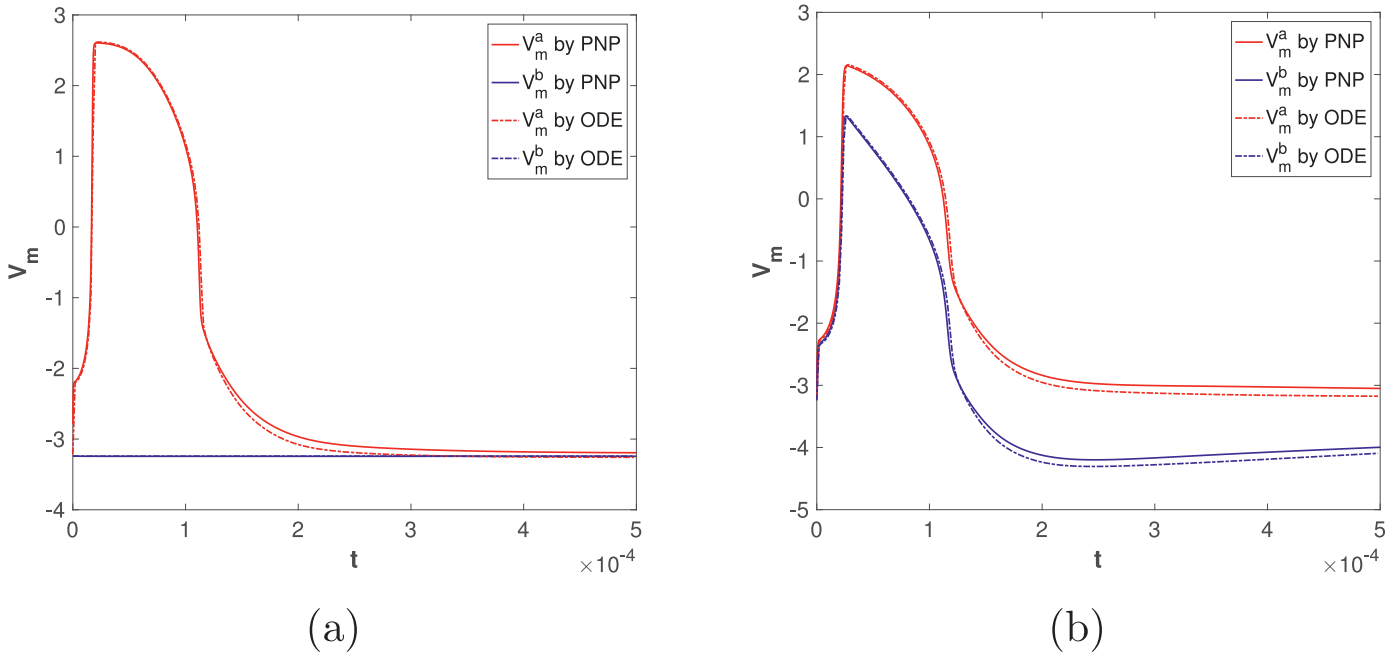

Fig. 10. Comparison of dynamics of two membrane potentials between ODE model (dashed lines) and PNP+resistor model (solid lines): (a) $\sigma = 0$, (b) $\sigma = 1$.

open circuit ($\sigma = 0$) and the closed circuit ($\sigma = 1$) cases, where the receptors are open to induce APs.

Since there are BLs near the membranes and the junctions between electrocyte and resistor, refined mesh are adopted in these regions to capture the profiles of concentrations and the electric potential. More precisely, we set a nonuniform mesh with mesh size $\Delta x = 3.0 \times 10^{-3}$ in the bulk region, which is gradually refined to $\Delta x = 1.7 \times 10^{-6}$ in BLs near $x = 0, a, b, 1$.

Fig. 4 (a) shows the dynamics of the two membrane potentials V_m^a and V_m^b, which reach the resting state soon, where the net current across the membrane is 0. The resting potentials are calculated as

$$V_m^a|_{t=5\times10^{-4}} = \psi_+^a - \psi_-^a = -3.2443,$$
$$V_m^b|_{t=5\times10^{-4}} = \psi_-^b - \psi_+^b = -3.2414, \quad (77)$$

and before scaling they are about -84 mV. Fig. 4(b) presents the profile of electric potential at time $t = 5 \times 10^{-4}$. It shows that the electric potential ψ is a constant in the bulk regions, and there are BLs on both sides of the membranes.

Starting from the resting state, ACh receptors are activated at the innervated membrane $x = a$, generating extra flux for sodium ion, thereby inducing an AP. We compare the two cases of open circuit with $\sigma = 0$ and closed circuit with $\sigma = 1$. Fig. 5 shows

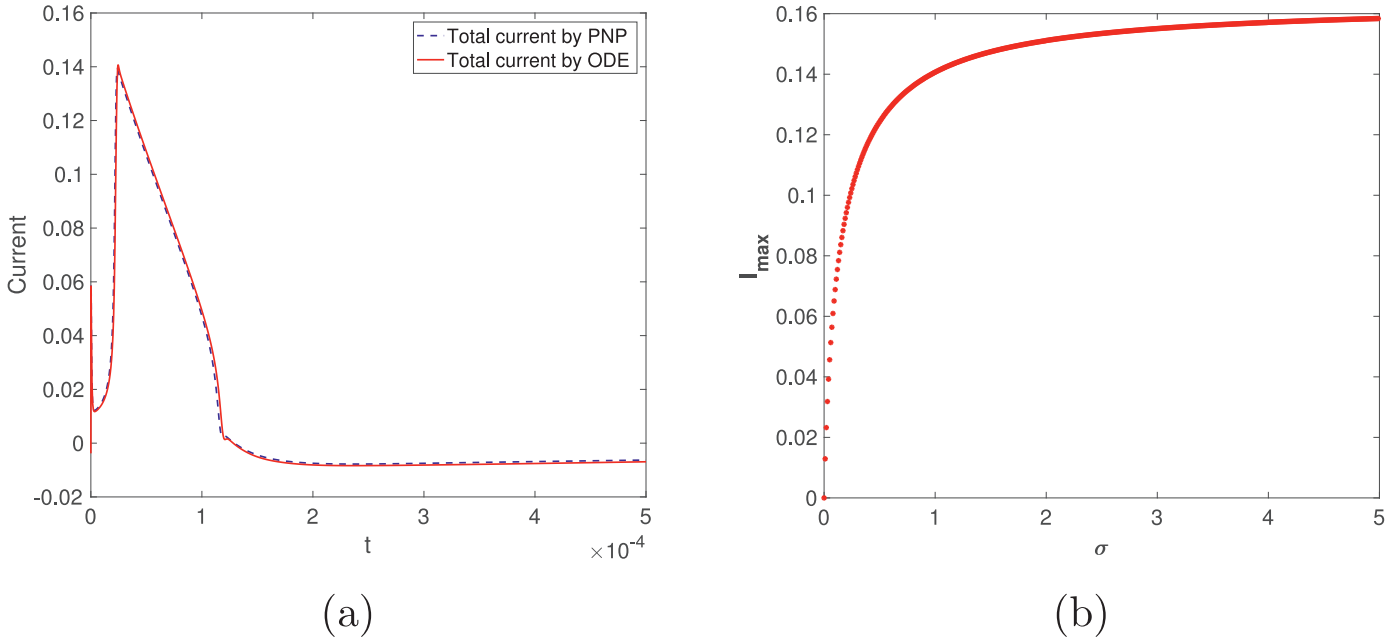

Fig. 11. (a) Comparison of the total current I^* between the ODE model (dashed line) and the PNP+resistor model (solid line) with $\sigma = 1$ (b) dependence of maximum total current $I_{\max}$ on σ by the ODE model.

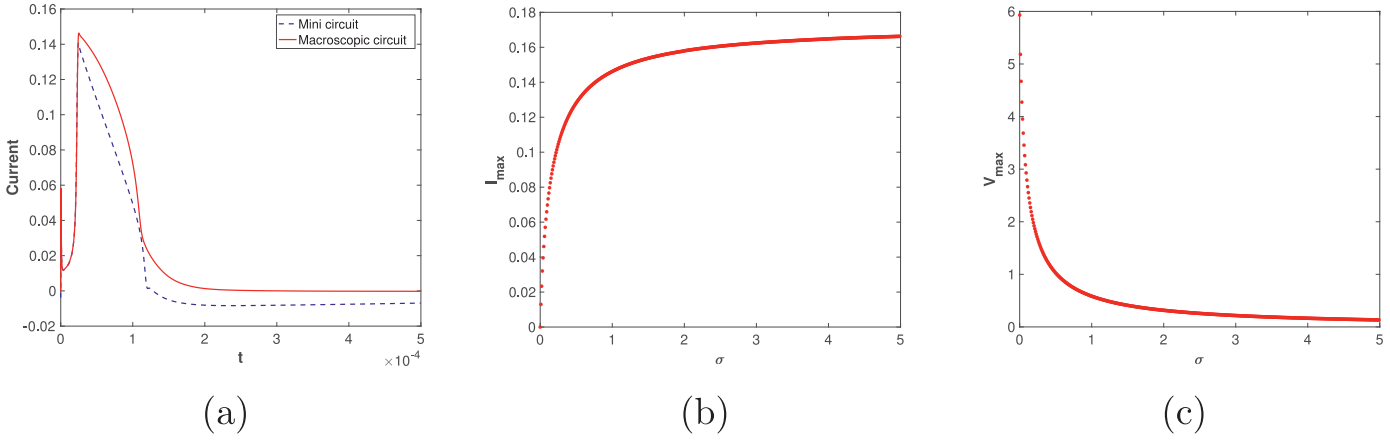

Fig. 12. (a) Comparison of Dynamics of the total current I^* between the macroscopic circuit model and the mini circuit model, (b) dependence of maximum total current $I_{\max}$ on σ by the macroscopic circuit model (c) dependence of maximum voltage $V_{\max}$ across one electrocyte on σ by the macroscopic circuit model.

the dynamics of membrane potentials V_m^a, V_m^b, and the total voltage (electric potential) difference over the entire electrocyte for the two cases. Fig. 5(a) recovers the result of open circuit in Cao et al. (2019) ($\sigma = 0$). It shows that an AP is generated at the innervated membrane from the curve of V_m^a, whereas the membrane potential V_m^b at the non-innervated membrane stays at the resting potential. Fig. 5(b) shows that APs are generated at both the innervated membrane and non-innervated membrane, induced by the current in the closed circuit. Figs. 5(c) and 5(d) show the total voltage difference over the entire electrocyte for the open and closed circuits, respectively. It can be seen that the built-up of electric potential in the closed circuit is less significant than that of the open circuit, and the maximum voltage difference for $\sigma = 1$ is roughly 1/10 of that for $\sigma = 0$.

The various currents and the total current on the two membranes are depicted in Fig. 6 for both cases $\sigma = 0$ and $\sigma = 1$. For the open circuit with $\sigma = 0$, Figs. 6(a) and 6(b) show the membrane currents on the right-hand side of (19), which are the same as those in Figs. 7(a) and 7(b) in Cao et al. (2019). The difference is that the total current here on membrane (the same as in the circuit) includes the induced current $I_E = -\epsilon^2 \partial_{tx} \psi$. The induced current is also shown in Fig. 6, and has significant values at certain time when V_m^a changes rapidly. With this new definition, the total current is essentially 0 during the dynamics. For the closed circuit with $\sigma = 1$, the currents on the right-hand side of (19), the induced current and the total current are shown in Figs. 6(c) and 6(d) respectively for innervated and non-innervated membranes. Compared with the case $\sigma = 0$, the scale of membrane currents at innervated membrane are similar, but the total current is significant, i.e., at the order $O(0.1)$. Since an AP is induced at non-innervated membrane in Fig. 5(b), the induced current and the total current there in Fig. 6(d) are also significant. The total current in Figs. 6(c) and 6(d) are the same, since it is preserved in the circuit.

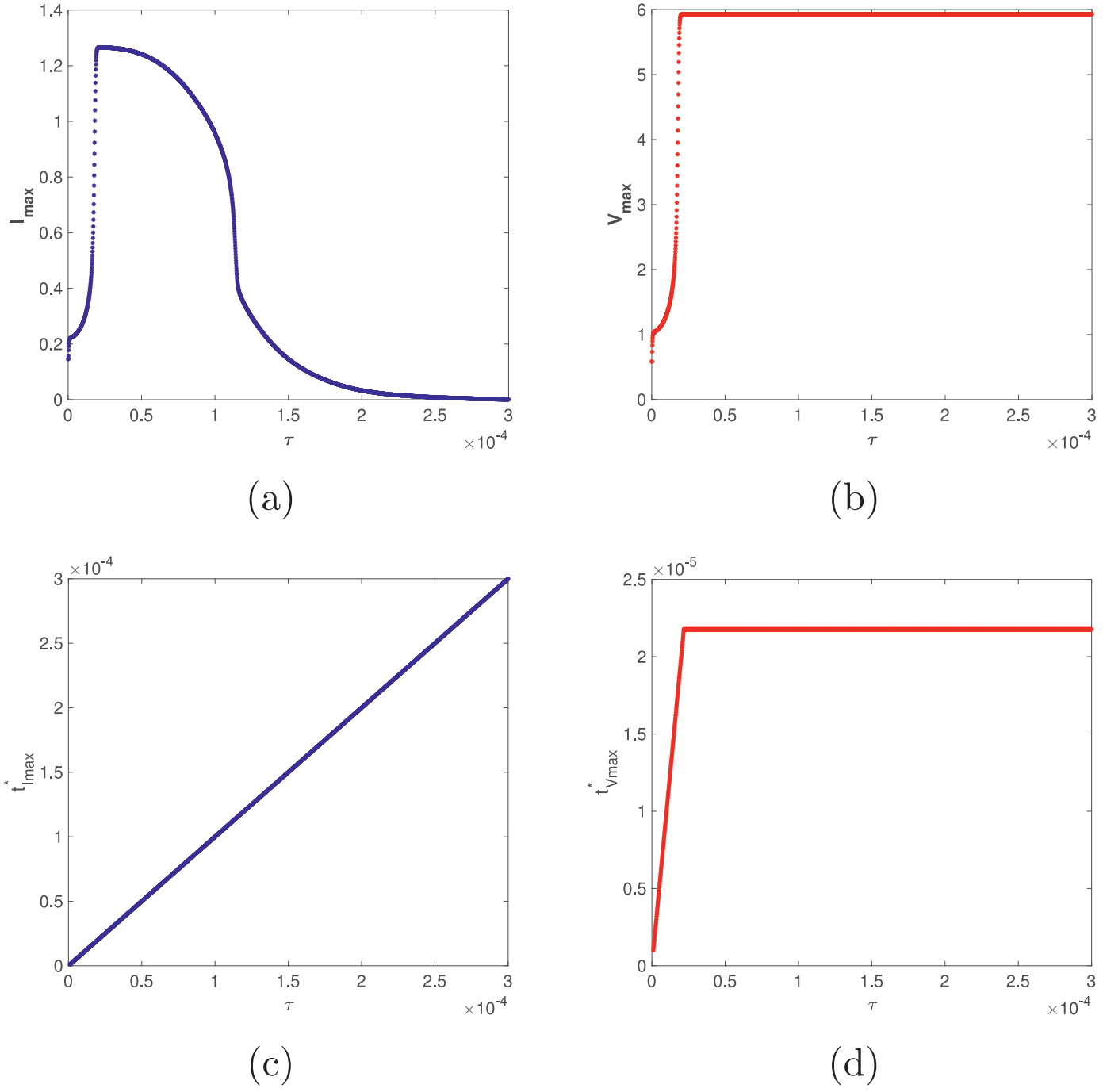

Fig. 13. (a) The dependence of maximum total current on the parameter τ, (b) the dependence of maximum voltage difference across one electrocyte on τ, (c) the dependence of t^*_{Imax} on τ, (d) the dependence of t^*_{Vmax} on τ.

Next, we present the profiles of concentrations and the electric potential for the case of the closed circuit at $t = 3 \times 10^{-5}$ (see Cao et al. (2019) for the case of the open circuit). Fig. 7 shows the profiles of concentrations c_i $(i = 1, 2, 3)$ for sodium, potassium and chloride. It shows that the concentrations are constants in bulk regions, and there are BLs near membranes $x = a, b$ and junction points $x = 0, 1$. The thickness of BLs is $O(\epsilon)$, and the variations in BLs near membranes are small (at order $O(C_m/\epsilon)$) while the variations are significant (at order $O(1)$) in BLs near junctions with resistor. These features are consistent with previous results in analysis. Fig. 8 shows the profile of the electric potential ψ. Fig. 8(a) shows that ψ behaves as a linear function in bulk, indicating a finite current in the circuit. Fig. 8(b) shows the BLs near membranes and junctions with resistor. Similar to the concentrations, the features of BLs agree with the analysis and estimates in Section 3. The BLs near junction $x = 0, 1$ appear because finite current is passed to the resistor through the term $\partial_{tx}\psi$.

Finally, we test the effect of different empirical models for currents I_i^b through the non-innervated membrane. Instead of the Goldman-Hodgkin-Katz (GHK) formulas $(A.8)_3$, we adopt an alternative HH type model in $(A.8)_4$. Fig. 9 compares the dynamics of the membrane potentials and the total current with GHK and HH

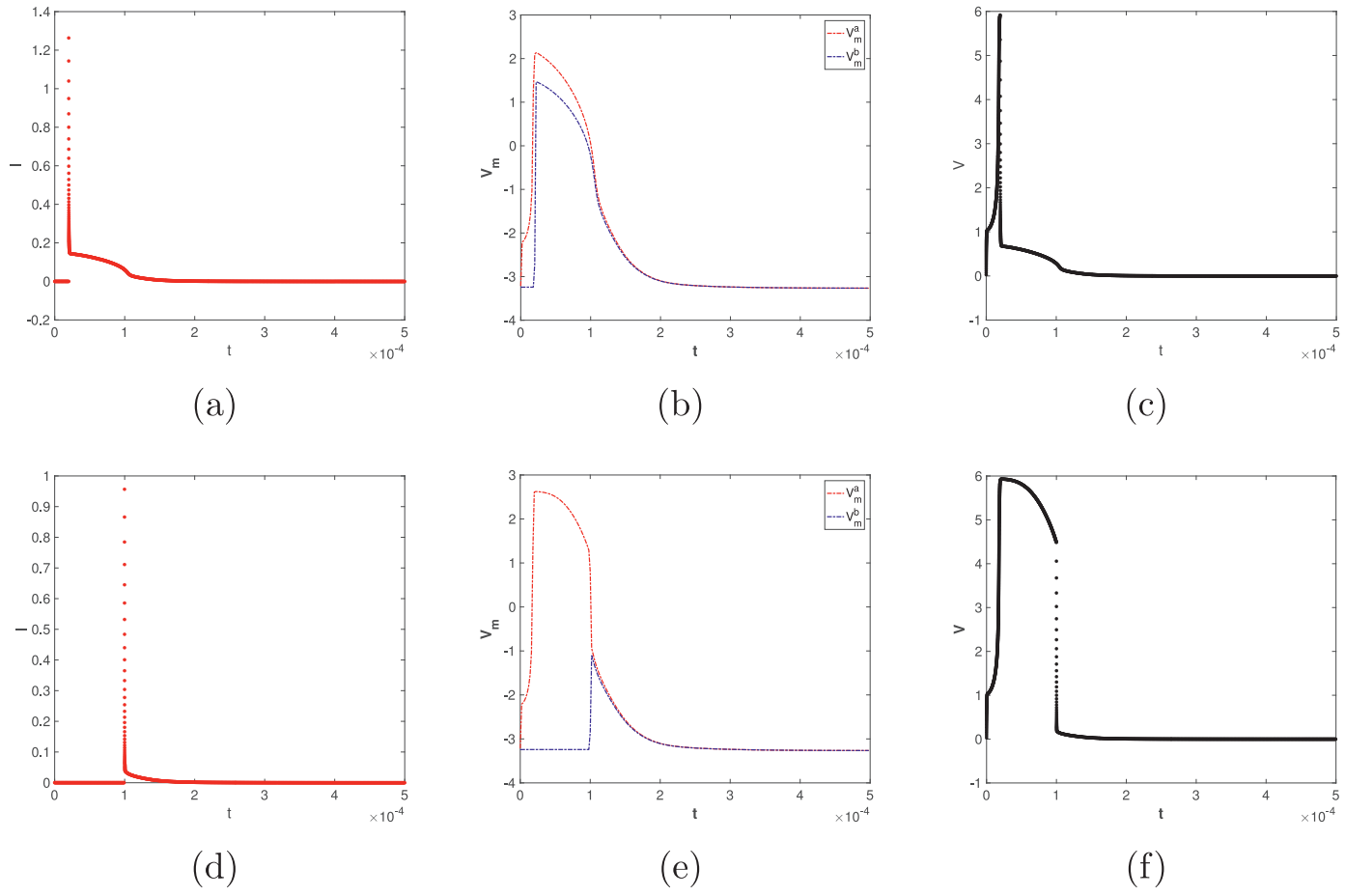

Fig. 14. The dynamics of total current, membrane potentials, and voltage across the electrocyte for two values of τ: (a)-(c) for $\tau = 0.2 \times 10^{-4}$ and (d)-(f) for $\tau = 1 \times 10^{-4}$.

models. They show similar profiles, revealing that the choice of empirical models has limited impact on the results.

4.2. The ODE model

In this subsection, we present the numerical results of the ODE models in (68,76). For validation, we compare the results of (68) with those in the preceding subsection. In addition, with the results from (76), we give an estimate for the total current in the macroscopic circuit.

Fig. 10 shows the dynamics of the two membrane potentials for both cases $\sigma = 0$ and $\sigma = 1$, where the solid lines are from the previous PNP model and dashed lines are from the ODE model in (68). The errors are small and the main features of the dynamics are captured.

Fig. 11 (a) compares the dynamics of the total current for the case $\sigma = 1$ between the ODE model (in dashed lines) and the PNP model (in solid lines). The error is negligible and the maximum total current during dynamics is about 0.14. Fig. 11(b) shows the dependence of the maximum total current $I_{\max}$ on the parameter σ, simulated by the ODE model. It shows that the maximum total current $I_{\max}$ increases as the conductance σ increases. The total current for the case $\sigma = 0$ is omitted here, since it is essentially 0 during dynamics.

Next, we give an estimate of the scale of the macroscopic total current and total voltage. Fig. 12(a) shows the dynamics of the total current by the ODE model in (76) with $\sigma = 1$ for the macroscopic circuit, compared with that in Fig. 11(a) for the mini-circuit. It shows similar trend, and gives the dimensionless maximum current value of about 0.15. The dependence of maximum current on parameter σ is presented in Fig. 12(b), which is similar to Fig. 11(b). By the parameter values in Appendix C, we get the scale for currents $I_0 = 118.74$ C/(s·m^2). If the contact area is of order 0.01 m^2, then we have the estimate for the dimensional maximum total current (with $\sigma = 1$)

$$I^{macro} \approx 0.15 \times 118.74 \times 0.01 \approx 0.18\text{A}. \tag{78}$$

Experiments show the total current is $O(0.1)$ in Amps (Catania, 2017a; 2017b; 2016), and the largest value reported in literature is roughly 1 A. Therefore, the present results are consistent with the scale of currents in experiments. Fig. 12(c) shows the voltage difference across one electrocyte by varying σ. The scale for voltage is 25.9 mV in Appendix C. When there are approximately 5000 electrocytes, the total voltage is estimated as

$$\begin{aligned} V^{macro} &\approx 0.59 \times 0.0259 \times 5000 \approx 76.4 \text{ V}, \quad \sigma = 1, \\ V^{macro} &\approx 5.9 \times 0.0259 \times 5000 \approx 764 \text{ V}, \quad \sigma = 0. \end{aligned} \tag{79}$$

As the total voltage is often measured in a separate experiment with an insulator in the circuit (Catania, 2016), the maximum values of total voltage should be compared with the case of $\sigma = 0$ or relatively small σ. The above scale is consistent with the data in experiments (Catania, 2017a; 2017b; 2016).

4.3. Maximum current

In the previous subsections, we have investigated in details of two special cases: open and closed circuits where either current or voltage across the electrocyte is small. In the case of a closed circuit, both membrane depolarizes, and as a result the voltage is not large. In the case of an open circuit, which can be considered as

the case when conductance is zero, only one membrane depolarizes which leads to a large voltage across the electrocyte but with no current generated. An interesting question is, therefore, whether it is possible to obtain a large voltage drop across the electrocyte with a large current.

In this section, we investigate the case when the contact between the eel and the prey is not made at the beginning and study the effect of the timing when the contact is made. From modeling point of view, this means that the conductance is a piecewise constant: $\sigma = 0$ for $t < \tau$ and $\sigma = 1$ for $t \geq \tau$ for some τ. Figs. 13(a) and 13 (b) show the maximum current and the maximum voltage difference (across one electrocyte) for various values of τ. It can be seen that both the maximum current and maximum voltage are significantly increased at about $\tau = 0.2 \times 10^{-4}$. The maximum current gradually decreases to 0 by further increase of τ whereas the maximum voltage stays as a constant.

This can be explained by the time delay between t^*_{Imax} and t^*_{Vmax} when the maximum values of current and voltage are achieved for certain values of τ, as shown in Figs. 13 (c) and 13(d). The two special cases with constants $\sigma = 1$ and $\sigma = 0$ correspond to the extreme cases when $\tau = 0$ and τ is relatively large (e.g., $\tau = 3 \times 10^{-4}$ in Fig. 13). The maximum voltage is small for $\tau = 0$ while the maximum current is small for large τ. On the other hand, for some intermediate values of τ, both large current and voltage can be obtained. Fig. 14 show the dynamics of the current, membrane potentials, and voltage across one electrocyte for two intermediate values of τ. In Fig. 14(a-c), with $\tau = 0.2 \times 10^{-4}$, both maximum current and voltage are large and both are achieved at $t = \tau$. In Figs. 14(d-f), with $\tau = 1 \times 10^{-4}$, the maximum current occurs at $t = \tau$ while the maximum voltage occurs at about $t = 0.2 \times 10^{-4}$.

5. Conclusions

In this paper, we have studied the electric discharge of electrocytes in electric eels. We focus on a model for a single electrocyte and a complete formulation is provided, including the Poisson-Nernst-Planck (PNP) system for the EC and IC spaces, various currents on membranes and Maxwell's formulation for the resistor. Using asymptotic analysis, we have derived simplified system with the PNP system replaced by ordinary differential equations (ODEs) that involves the dynamics of two membrane potentials and preserves the total current in the closed electric circuit. The features and estimates in our analysis have been validated in numerical results of both PNP and ODE models. On the organ scale, a macroscopic circuit model is also derived based on the single electrocyte model, which justifies the circuit models in the literature. Our estimate of the total current is consistent with the values reported in various experiments.

CRediT authorship contribution statement

Zilong Song: Formal analysis, Writing - original draft. **Xiulei Cao:** Conceptualization, Writing - original draft. **Tzyy-Leng Horng:** Writing - original draft. **Huaxiong Huang:** Methodology, Writing - original draft.

Acknowledgments

This work is supported in part by the Natural Science and Engineering Research Council (NSERC) of Canada, the Fields Institute for Research in Mathematical Sciences and the National Center for Theoretical Sciences of Taiwan. The authors would like to thank Shixin Xu and other members of the Fields CQAM Lab on Health Analytics and Multidisciplinary Modeling for helpful comments and suggestions.

Appendix A. Formulas for currents on membranes

At the innervated membrane $x = a$, the currents through the voltage-gated channels (positive from intracellular region to extracellular region) are given by the HH model (Malmivuo and Plonsey, 1995; Hodgkin and Huxley, 1990)

$$I_i^{VG} = G_i(V_m^a - V_i^a) = G_i\left(\psi_+^a - \psi_-^a - \frac{k_B T}{z_i e_0} \ln \frac{c_{i,-}^a}{c_{i,+}^a}\right), \quad i = 1, 2, 3, \tag{A.1}$$

where V_i^a are the Nernst potentials for ion species c_i defined by the last term in brackets, G_i are the conductances and given by Xu and Lavan (2008)

$$G_1 \equiv \bar{g}_{Na} m^3\ h + \bar{g}_{Na,leak}, \quad G_2 \equiv \bar{g}_K n^4 + \bar{g}_{K,leak}, \quad G_3 \equiv \bar{g}_{Cl}, \tag{A.2}$$

where $\bar{g}_{Na}, \bar{g}_K, \bar{g}_{Cl}, \bar{g}_{Na,leak}, \bar{g}_{K,leak}$ are constants, and m, h, n are the gating variables whose dynamics depend on the membrane potential V_m^a (see Appendix B). The current from Kir channel is given by Xu and Lavan (2008) and Nygren et al. (1998)

$$I_2^{Kir} = \frac{\bar{g}_{Kir}(V_m^a - V_2^a)}{1 + e^{\frac{n_1 F}{RT}(V_m^a - V_2^a + n_2)}}, \tag{A.3}$$

where $\bar{g}_{Kir}$ is the maximum conductance, and n_1 and n_2 are the two parameters. There are currents I_1^R and I_2^R for Na^+ and K^+ through receptors, but only the total current of the two are measured experimentally (Chakrapani et al., 2004; Adams, 1981; Mitra et al., 2005) and previous work (Cao et al., 2019) showed that only the total current matters and there is little difference for different combinations of the two currents. We set (Cao et al., 2019)

$$I_1^R = I_1^*, \quad I_2^R = 0, \tag{A.4}$$

where I_1^* is given by Sheridan and Lester (1977), Magleby and Stevens (1972), Xu and Lavan (2008)

$$I_1^* = \frac{[A]^2 \bar{g}_R e^{-\alpha t}}{[A]^2 + 2[A]\frac{k_{-2}}{k_{+2}} + \frac{k_{-1}k_{-2}}{k_{+1}k_{+2}}}(V_m^a - V_0), \quad 2k_{-2} = \alpha = \alpha_0 e^{\frac{V_m^a}{V_1}}, \tag{A.5}$$

where [A] is the concentration of agonist, $\bar{g}_R$ is the conductance and V_0, V_1, α_0 are parameters.

At the non-innervated membrane $x = b$, we consider two cases for the currents through the channels. First, as in previous work Cao et al. (2019), the current is described by the Goldman-Hodgkin-Katz (GHK) model Xu and Lavan (2008) and Hille et al. (2001)

$$I_i^b = P_i z_i^2 \frac{V_m^b F^2 \left(c_{i,-}^b - c_{i,+}^b e^{-\frac{z_i F}{RT} V_m^b}\right)}{RT\left(1 - e^{-\frac{z_i F}{RT} V_m^b}\right)}, \quad i = 1, 2, 3, \tag{A.6}$$

where P_i are the permeabilities. Second, the current is described by the HH-type model

$$I_i^b = G_i^b(V_m^b - V_i^b) = G_i^b\left(\psi_-^b - \psi_+^b - \frac{k_B T}{z_i e_0} \ln \frac{c_{i,+}^b}{c_{i,-}^b}\right), \quad i = 1, 2, 3, \tag{A.7}$$

where G_i^b are fixed conductances. The pumps I_i^{pump} are set as 0 in the simulation, since they have little impact on the fact AP dynamics and electric discharge. It restores the equilibrium state over a much longer timeframe.

The associated dimensionless formulas are given by

$$I_i^{VG} = G_i\left(V_m^a - \frac{1}{z_i} \ln \frac{c_{i,-}^a}{c_{i,+}^a}\right), \quad V_i^a = \frac{1}{z_i} \ln \frac{c_{i,-}^a}{c_{i,+}^a}$$

$$I_2^{Kir} = \frac{\bar{g}_{Kir}(V_m^a - V_2^a)}{1 + e^{n_1(V_m^a - V_2^a + n_2)}},$$

$$I_i^b = P_i z_i^2 \frac{V_m^b\left(c_{i,-}^b - c_{i,+}^b e^{-z_i V_m^b}\right)}{(1-e^{-z_i V_m^b})},$$
$$I_i^b = G_i^b (V_m^b - V_i^b), \quad V_i^b = \frac{1}{z_i}\ln\frac{c_{i,+}^b}{c_{i,-}^b} \tag{A.8}$$

and I_1^* remains the same form.

All the dimensional and dimensionless parameters in the formulas are given in Appendix C.

Appendix B. The dynamic system of *m, n, h*

The dynamic system of m, n, h is

$$\frac{dn}{dt} = \alpha_n(1-n) - \beta_n n,$$
$$\frac{dm}{dt} = \alpha_m(1-m) - \beta_m m,$$
$$\frac{dh}{dt} = \alpha_h(1-h) - \beta_h h. \tag{B.1}$$

The coefficients are given by

$$\alpha_n = 2.38\times 10^3 \cdot e^{\frac{V_m^a+0.0163}{0.0472}}, \quad \beta_n = 1.71\times 10^3 \cdot e^{-\frac{V_m^a+0.0164}{0.0184}}$$
$$\alpha_m = 2.64\times 10^4 \cdot e^{\frac{V_m^a+0.0618}{0.0295}}, \quad \beta_m = 2.59\times 10^4 \cdot e^{-\frac{V_m^a+0.0618}{0.0242}}$$
$$\alpha_h = 1.08\times 10^3 \cdot e^{-\frac{V_m^a+0.0545}{0.00784}},$$
$$\beta_h = 1.49\times 10^3/(0.0745 + e^{-\frac{V_m^a+0.0545}{0.0129}}), \tag{B.2}$$

where V_m^a are dimensional values in unit Volt, and α_i and β_i ($i = n, m, h$) are dimensionless parameters already scaled by diffusion time scale. With $V_m^a = -0.084$ V, we obtain the steady state solution

$$n_0 = 0.008458, \quad m_0 = 0.1622, \quad h_0 = 0.9967, \tag{B.3}$$

which are used as initial values in simulations of electric discharge.

Appendix C. The parameters and data

The data are mainly from Hodgkin and Huxley (1990), Pods et al. (2013), Sheridan and Lester (1977), Magleby and Stevens (1972), and Cao et al. (2019) and the book in Liu and Eisenberg (2014). The constants are

$$k_B = 1.38\times 10^{-23}\text{J/K} \quad N_A = 6.022\times 10^{23}/\text{mol},$$
$$e_0 = 1.602\times 10^{-19}\text{C} \quad \epsilon_0 = 8.854\times 10^{-12}\text{C}/(\text{V}\cdot\text{m}),$$
$$T = 300.15\,\text{K}, \quad F = e_0 N_A \quad R = k_B N_A.$$

Some typical values are

$$\epsilon_r = 80, \quad \epsilon_r^m = 2, \quad c_0 = 160\,\text{mM} = 160\,\text{mol/m}^3,$$
$$h_m = 5\,\text{nm}, \quad L = 130\ \mu\text{m}, \quad a = 25\ \mu\text{m}, \quad b = 105\ \mu\text{m},$$
$$D_0 = 10^{-9}\,\text{m}^2/\text{s}, \quad D_1 = 1.33D_0, \quad D_2 = 1.96D_0, \quad D_3 = 2.03D_0. \tag{C.1}$$

The conductances and parameters in flux formulas are given by

$$\bar g_{Na} = 157\,\text{mS/cm}^2 = 1570\,\text{C}/(\text{V}\cdot\text{s}\cdot\text{m}^2),$$
$$\bar g_K = 320\,\text{C}/(\text{V}\cdot\text{s}\cdot\text{m}^2), \quad \bar g_{Cl} = 0\,\text{C}/(\text{V}\cdot\text{s}\cdot\text{m}^2),$$
$$\bar g_{Na,leak} = 0.2761\,\text{C}/(\text{V}\cdot\text{s}\cdot\text{m}^2) \quad \bar g_{K,leak} = 31.5390\,\text{C}/(\text{V}\cdot\text{s}\cdot\text{m}^2),$$
$$\bar g_{Kir} = 591\,\text{C}/(\text{V}\cdot\text{s}\cdot\text{m}^2), \quad \bar g_R = 700\,\text{C}/(\text{V}\cdot\text{s}\cdot\text{m}^2),$$
$$P_1 = 0, \quad P_2 = 1.12\times 10^{-6}\text{m/s}, \quad P_3 = 7.63\times 10^{-8}\text{m/s},$$
$$G_1^b = 0, \quad G_2^b = 869\,\text{C}/(\text{V}\cdot\text{s}\cdot\text{m}^2), \quad G_3^b = 2.28\,\text{C}/(\text{V}\cdot\text{s}\cdot\text{m}^2),$$
$$n_1 = 1.45, \quad n_2 = -0.0630\,\text{V}, \quad [A] = 0.1\text{mol/m}^3,$$
$$V_0 = 0, \quad V_1 = 125.79\ \text{mV},$$
$$\alpha_0 = 1.67\ \text{ms}^{-1} = 1.67\times 10^3\ \text{s}^{-1},$$
$$k_{+2} = 7\times 10^6\ \text{m}^3/(\text{mol}\cdot\text{s}), \quad k_{-1}/k_{+1} = 2\times 10^{-2}\ \text{mol/m}^3. \tag{C.2}$$

From the data, we get the scales

$$\frac{k_B T}{e_0} = 25.9\,\text{mV}, \quad \frac{L^2}{D_0} = 16.9\,\text{s}, \quad \lambda_D = 1.09\times 10^{-9}\ \text{m},$$
$$G_0 = 4592.2\,\text{C}/(\text{V}\cdot\text{s}\cdot\text{m}^2), \quad P_0 = 7.69\times 10^{-6}\ \text{m/s},$$
$$I_0 = 118.74\ \text{C}/(\text{s}\cdot\text{m}^2), \quad \sigma_0 = 0.6/(\Omega\cdot\text{m}). \tag{C.3}$$

The constants in dimensionless system are

$$\epsilon = 8.38\times 10^{-6}, \quad \epsilon_m = 1.32\times 10^{-6},$$
$$h_m = 3.85\times 10^{-5}, \quad a = 0.1923, \quad b = 0.8077,$$
$$D_1 = 1.33, \quad D_2 = 1.96, \quad D_3 = 2.03, \quad q = -0.4478,$$
$$\alpha_0 = 2.82\times 10^4, \quad n_1 = 1.45, \quad n_2 = -2.4366,$$
$$\bar g_{Na} = 0.3419, \quad \bar g_K = 0.06968, \quad \bar g_{Cl} = 2.18\times 10^{-4},$$
$$\bar g_{Na,leak} = 6.0123\times 10^{-5} \quad \bar g_{K,leak} = 6.8679\times 10^{-3},$$
$$\bar g_{Kir} = 0.1287, \quad \bar g_R = 0.1524, \quad V_0 = 0, \quad V_1 = 4.86,$$
$$[A] = 6.25\times 10^{-4}, \quad k_{+2} = 1.89\times 10^7,$$
$$k_{-1}/k_{+1} = 1.25\times 10^{-4},$$
$$P_1 = 0, \quad P_2 = 0.1455, \quad P_3 = 0.009914,$$
$$G_1^b = 0, \quad G_2^b = 0.01893, \quad G_3^b = 4.9595\times 10^{-4}. \tag{C.4}$$

Appendix D. Derivation in Section 3.2

For derivations of 59–(61), we take the membrane at $x = a$ for example. For EC space, based on the BL analysis in Song et al. (2018a) (see Eq. (29) therein), we get

$$\tfrac{C_m}{\epsilon}(\psi_+^a - \psi_-^a) = -\text{sign}(\psi_L^a - \psi_-^a)\sqrt{2\textstyle\sum_{i=1}^3 c_{iL}^a\left(e^{z_i(\psi_L^a-\psi_-^a)} - 1\right)}. \tag{D.1}$$

where in this problem we can set the limit values of bulk concentrations at membrane as $c_{iL}^a = c_{iE}$. For the IC space, there is nonzero permanent charge q, we can slightly modify the BL analysis. With $X = (x-a)/\epsilon$ in BL, we get at leading order

$$\epsilon^2\,(\partial_x\psi)^2\big|_{x=a+} = (\partial_X\psi)^2\big|_{X=0} = 2\sum_{i=1}^3 c_{iR}^a\left(e^{z_i(\psi_R^a-\psi_+^a)} - 1\right) + 2q(\psi_R^a - \psi_+^a), \tag{D.2}$$

Removing the square root, setting $c_{iR}^a = c_{iI}$, and using the condition $(22)_1$, we get

$$\tfrac{C_m}{\epsilon}V_m^a = \text{sign}(\psi_R^a - \psi_+^a)\sqrt{2\textstyle\sum_{i=1}^3 c_{iI}\left(e^{z_i(\psi_R^a-\psi_+^a)} - 1\right) + 2q(\psi_R^a - \psi_+^a)}. \tag{D.3}$$

Based on the parameter values, one can easily get

$$O\left(\frac{C_m}{\epsilon}\right) \sim 10^{-2}, \tag{D.4}$$

which implies the variations $\psi_R^a - \psi_+^a$ and $\psi_L^a - \psi_-^a$ are small and at the above order, thus

$$V_m^a = \psi_+^a - \psi_-^a \approx \tilde V_m^a = \psi_R^a - \psi_L^a. \tag{D.5}$$

By keeping up to $O(C_m/\epsilon)$ terms, i.e., expanding the right-hand side of (D.1,D.3) together with electro-neutrality, we get

$$\frac{C_m}{\epsilon}V_m^a = -\sqrt{\sum_{i=1}^3 z_i^2 c_{iE}}(\psi_L^a - \psi_-^a), \quad \frac{C_m}{\epsilon}V_m^a = \sqrt{\sum_{i=1}^3 z_i^2 c_{iI}}(\psi_R^a - \psi_+^a). \tag{D.6}$$

Substituting the valences and by definitions of $V_m^a, \tilde{V}_m^a$, we get

$$\tilde{V}_m^a = V_m^a + (\psi_R^a - \psi_+^a) - (\psi_L^a - \psi_-^a) \tag{D.7}$$

$$= V_m^a\left(1 + \frac{C_m}{\epsilon}\frac{1}{\sqrt{c_{1I}+c_{2I}+c_{3I}}} + \frac{C_m}{\epsilon}\frac{1}{\sqrt{c_{1E}+c_{2E}+c_{3E}}} + o(\frac{C_m}{\epsilon})\right). \tag{D.7}$$

By using electro-neutrality condition $c_{1E}+c_{2E}=c_{3E}$, moving the factor to the left-hand side and keeping the equivalent order at $O(C_m/\epsilon)$, we obtain (60). Following a similar procedure, we get the result for V_m^b in (60). For formulas in (61), we take $c_{i,-}^a$ for example, others are similarly derived. By the BL analysis, we get

$$c_{i,-}^a = c_{iL}^a e^{-z_i(\psi_-^a - \psi_L^a)} = c_{iE} e^{z_i(\psi_L^a - \psi^a)}. \tag{D.8}$$

Combining with (D.6,D.7) and electro-neutrality $c_{1E}+c_{2E}=c_{3E}$, we get up to the order $O(C_m/\epsilon)$ that

$$c_{i,-}^a = c_{iE}\left(1 + z_i(\psi_L^a - \psi_-^a)\right) = c_{iE}\left(1 - \frac{C_m}{\epsilon}\frac{z_i V_m^a}{\sqrt{2c_{3E}}}\right)$$

$$= c_{iE}\left(1 - \frac{C_m}{\epsilon}\frac{z_i \tilde{V}_m^a}{\sqrt{2c_{3E}}}\right). \tag{D.9}$$

For BL near $x=1$, since fluxes are $O(1)$ in bulk and the fluxes are 0 at $x=1$, the fluxes are at most $O(1)$ in BL, then there is a standard BL. This is similar to BL at membranes, and the only difference is that the variation of ψ is relatively large, i.e., at $O(1)$ when the total current is finite. With the scaling $X=(1-x)/\epsilon$ in BL and $q=0$ in EC space, we get at leading order

$$\epsilon^2 (\partial_x \psi)^2\big|_{x=1-} = (\partial_X \psi)^2\big|_{X=0} = 2\sum_{i=1}^{3} c_{iL}^1\left(e^{-z_i(\psi_-^1 - \psi_L^1)} - 1\right). \tag{D.10}$$

By setting $c_{iL}^1 = c_{iE}$, using definition $V_1^{BL} = \psi_-^1 - \psi_L^1$ and taking the square root, we get

$$\epsilon\,\partial_x\psi|_{x=1-} = \mathrm{sign}(V_1^{BL})\sqrt{2(c_{1E}+c_{2E})(e^{-V_1^{BL}}-1) + 2c_{3E}(e^{V_1^{BL}}-1)}$$

$$= \mathrm{sign}(V_1^{BL})\sqrt{2c_{3E}(e^{-V_1^{BL}} + e^{V_1^{BL}} - 2)}$$

$$= \sqrt{2c_{3E}}(e^{V_1^{BL}/2} - e^{-V_1^{BL}/2}). \tag{D.11}$$

References

Adams, P., 1981. Acetylcholine receptor kinetics. J. Membr. Biol. 58 (3), 161–174.
Bauer, R., 1979. Electric organ discharge (eod) and prey capture behaviour in the electric eel, electrophorus electricus. Behav. Ecol. Sociobiol. (Print) 4 (4), 311–319.
Bennett, M.V., 1961. Modes of operation of electric organs. Ann. N. Y. Acad. Sci. 94 (2), 458–509.
Bennett, M.V., 1970. Comparative physiology: electric organs. Annu. Rev. Physiol. 32 (1), 471–528.
Bezanilla, F., 2007. Voltage-gated Ion Channels. In: Biological Membrane Ion Channels. Springer, pp. 81–118.
Brown, M., 1950. The electric discharge of the electric eel. Electr. Eng. 69 (2), 145–147.
Campenot, R.B., 2016. Animal Electricity. Harvard University Press.
Cao, X., Song, Z., Horng, T.-L., Huang, H., 2019. Electric potential generation of electrocytes: modelling, analysis, and computation. J. Theor. Biol. 110107.
Carlson, B.A., 2015. Animal behavior: electric eels amp up for an easy meal. Curr. Biol. 25 (22), R1070–R1072.
Catania, K., 2014. The shocking predatory strike of the electric eel. Science 346 (6214), 1231–1234.
Catania, K.C., 2015. Electric eels concentrate their electric field to induce involuntary fatigue in struggling prey. Current Biol. 25 (22), 2889–2898.
Catania, K.C., 2015. Electric eels use high-voltage to track fast-moving prey. Nat Commun 6, 8638.
Catania, K.C., 2015. An optimized biological taser: electric eels remotely induce or arrest movement in nearby prey. Brain Behav. Evol. 86 (1), 38–47.
Catania, K.C., 2016. Leaping eels electrify threats, supporting humboldt's account of a battle with horses. Proc. Natl. Acad. Sci. 113 (25), 6979–6984.
Catania, K.C., 2017. Electrical potential of leaping eels. Brain Behav. Evol. 89 (4), 262–273.
Catania, K.C., 2017. Power transfer to a human during an electric eel's shocking leap. Curr. Biol. 27 (18), 2887–2891.
Chakrapani, S., Bailey, T.D., Auerbach, A., 2004. Gating dynamics of the acetylcholine receptor extracellular domain. J. Gen. Physiol. 123 (4), 341–356.
Coates, C., 1950. Electric fishes. Electr. Eng. 69 (1), 47–51.
Dunlap, K.D., McAnelly, M.L., Zakon, H.H., 1997. Estrogen modifies an electrocommunication signal by altering the electrocyte sodium current in an electric fish, sternopygus. J. Neurosci. 17 (8), 2869–2875.
Eisenberg, R.S., Gold, N., Song, Z., Huang, H., 2018. What current flows through a resistor? arXiv preprint arXiv:1805.04814.
Eisenberg, R.S., Oriols, X., Ferry, D., 2017. Dynamics of current, charge and mass. Comput. Math. Biophys. 5 (1), 78–115.
Finger, S., Piccolino, M., 2011. The Shocking History of Electric Fishes: From Ancient Epochs to the Birth of Modern Neurophysiology. Oxford University Press.
Gotter, A.L., Kaetzel, M.A., Dedman, J.R., 1998. Electrophorus electricus as a model system for the study of membrane excitability. Compar. Biochem. Physiol. Part A 119 (1), 225–241.
Hille, B., et al., 2001. Ion Channels of Excitable Membranes, Vol. 507. Sinauer Sunderland, MA.
Hodgkin, A., Huxley, A., 1990. A quantitative description of membrane current and its application to conduction and excitation in nerve. Bull. Math. Biol. 52 (1–2), 25–71.
Hodgkin, A.L., Huxley, A.F., 1952. A quantitative description of membrane current and its application to conduction and excitation in nerve. J. Physiol. (Lond.) 117 (4), 500–544.
Horowitz, P., Hill, W., 2015. The art of electronics, 193, 204.
Humayun, M.S., Weiland, J.D., Fujii, G.Y., Greenberg, R., Williamson, R., Little, J., Mech, B., Cimmarusti, V., Van Boemel, G., Dagnelie, G., et al., 2003. Visual perception in a blind subject with a chronic microelectronic retinal prosthesis. Vision Res. 43 (24), 2573–2581.
Jackson, J. D., 1999. Classical electrodynamics.
Keynes, R., Martins-Ferreira, H., 1953. Membrane potentials in the electroplates of the electric eel. J. Physiol. (Lond.) 119 (2–3), 315–351.
Kilic, M.S., Bazant, M.Z., Ajdari, A., 2007. Steric effects in the dynamics of electrolytes at large applied voltages. i. double-layer charging. Phys. Rev. E 75 (2), 21502.
Kilic, M.S., Bazant, M.Z., Ajdari, A., 2007. Steric effects in the dynamics of electrolytes at large applied voltages. ii. modified poisson-nernst-planck equations. Phys. Rev. E 75 (2), 21503.
Lissmann, H., 1958. On the function and evolution of electric organs in fish. J. Exp. Biol. 35 (1), 156–191.
Liu, J.-L., Eisenberg, R.S., 2014. Poisson-nernst-planck-fermi theory for modeling biological ion channels. J Chem Phys 141 (22), 12B640_1.
Liu, W., 2009. One-dimensional steady-state poisson–nernst–planck systems for ion channels with multiple ion species. J Differ Equ 246 (1), 428–451.
Maciver, M.A., Sharabash, N.M., Nelson, M.E., 2001. Prey-capture behavior in gymnotid electric fish: motion analysis and effects of water conductivity. J. Exp. Biol. 204 (3), 543–557.
Magleby, K., Stevens, C., 1972. The effect of voltage on the time course of end-plate currents. J. Physiol. (Lond.) 223 (1), 151–171.
Malmivuo, J., Plonsey, R., 1995. Bioelectromagnetism: Principles and Applications of Bioelectric and Biomagnetic Fields. Oxford University Press, USA.
Markham, M.R., 2013. Electrocyte physiology: 50 years later. J. Exp. Biol. 216 (13), 2451–2458.
Mauro, A., 1969. The role of the voltaic pile in the galvani-volta controversy concerning animal vs. metallic electricity. J Hist Med Allied Sci 24 (2), 140–150.
Mitra, A., Cymes, G.D., Auerbach, A., 2005. Dynamics of the acetylcholine receptor pore at the gating transition state. Proc. Natl. Acad. Sci. 102 (42), 15069–15074.
Moller, P., 1995. Electric fishes: History and Behavior, Vol. 17. Springer.
Mori, Y., Liu, C., Eisenberg, R.S., 2011. A model of electrodiffusion and osmotic water flow and its energetic structure. Physica D 240 (22), 1835–1852.
Nelson, J.S., Grande, T.C., Wilson, M.V., 2016. Fishes of the World. John Wiley & Sons.
Noda, M., Shimizu, S., Tanabe, T., Takai, T., Kayano, T., Ikeda, T., Takahashi, H., Nakayama, H., Kanaoka, Y., Minamino, N., et al., 1984. Primary structure of electrophorus electricus sodium channel deduced from cdna sequence. Nature 312 (5990), 121.
Nygren, A., Fiset, C., Firek, L., Clark, J., Lindblad, D., Clark, R., Giles, W., 1998. Mathematical model of an adult human atrial cell: the role of k+ currents in repolarization. Circ. Res. 82 (1), 63–81.
Pods, J., 2017. A comparison of computational models for the extracellular potential of neurons. J. Integr. Neurosci. 16 (1), 19–32.
Pods, J., Schönke, J., Bastian, P., 2013. Electrodiffusion models of neurons and extracellular space using the poisson-nernst-planck equations-numerical simulation of the intra-and extracellular potential for an axon model. Biophys. J. 105 (1), 242–254.
Rubinstein, I., 1990. Electro-diffusion of ions. SIAM.
Schmuck, M., Bazant, M.Z., 2015. Homogenization of the poisson–nernst–planck equations for ion transport in charged porous media. SIAM J Appl Math 75 (3), 1369–1401.
Schroeder, T.B., Guha, A., Lamoureux, A., VanRenterghem, G., Sept, D., Shtein, M., Yang, J., Mayer, M., 2017. An electric-eel-inspired soft power source from stacked hydrogels. Nature 552 (7684), 214.
Sheridan, R.E., Lester, H.A., 1977. Rates and equilibria at the acetylcholine receptor of electrophorus electroplaques. a study of neurally evoked postsynaptic currents and of voltage-jump relaxations. J. Gen. Physiol. 70 (2), 187.
Song, Z., Cao, X., Horng, T.-L., Huang, H., 2019. Selectivity of the kcsa potassium channel: analysis and computation. Phys. Rev. E 100 (2), 22406.
Song, Z., Cao, X., Huang, H., 2018. Electroneutral models for a multidimensional dynamic poisson-nernst-planck system. Phys. Rev. E 98 (3), 32404.

Song, Z., Cao, X., Huang, H., 2018. Electroneutral models for dynamic poisson-nernst-planck systems. Phys. Rev. E 97 (1), 12411.
Sun, H., Fu, X., Xie, S., Jiang, Y., Peng, H., 2016. Electrochemical capacitors with high output voltages that mimic electric eels. Adv. Mater. 28 (10), 2070–2076.
Westby, G.M., 1988. The ecology, discharge diversity and predatory behaviour of gymnotiforme electric fish in the coastal streams of french guiana. Behav. Ecol. Sociobiol. (Print) 22 (5), 341–354.
Xu, J., Lavan, D.A., 2008. Designing artificial cells to harness the biological ion concentration gradient. Nat Nanotechnol 3 (11), 666.